ACS OMEGA

Open Access

http://pubs.acs.org/journal/acsodf

Article

Properties of Mixed Crystal Coprecipitation Substances of Ammonium Nitrate and Potassium Perchlorate Prepared by the Evaporative Solvent Method

Rongcai Zi, Zhiyue Han,* Yue Yu, Cheng Wang, Ximing Zhang, Xueyong Guo, Jianhua Chen, Xinrui Zhang, and Jun Yang

Cite This: *ACS Omega* 2024, 9, 1573−1590

Read Online

ACCESS | Metrics & More | Article Recommendations

ABSTRACT: Ammonium perchlorate (AP) has been widely used as an oxidizer in propellants and military mixed explosives in recent years. However, its high characteristic signal, environmental pollution, and poor detonation performance have prompted the industry to seek alternatives to AP. Ammonium nitrate (AN) is a suitable substitute due to its low characteristic signal, lack of pollution, and excellent detonation performance. However, its room-temperature phase transition and hygroscopicity affect its practical use. In this work, we prepared mixed crystal coprecipitation (MCC) materials of AN and potassium perchlorate (KP) using the evaporative solvent method. The characterization of AN/KP MCCs was carried out by combining TG-DSC, XRD, FT-IR, and SEM analysis, revealing that the formation of MCCs by AN and KP is due to ion exchange between the two components. AN/KP MCCs not only solve the problem of room-temperature phase transition in AN but also reduce its hygroscopicity. Furthermore, AN/KP MCCs have mechanical sensitivity, explosive performance, and specific impulse similar to pure AN, but compared to AN, AN/KP MCCs have higher density, effective oxygen content, and thermal stability. Compared with existing oxidizers AN, AP, and KP, AN/KP MCCs with high density, low sensitivity, high oxygen content, and high safety have obvious advantages and have good prospects in the application of oxidizers in solid propellants and military mixed explosives.

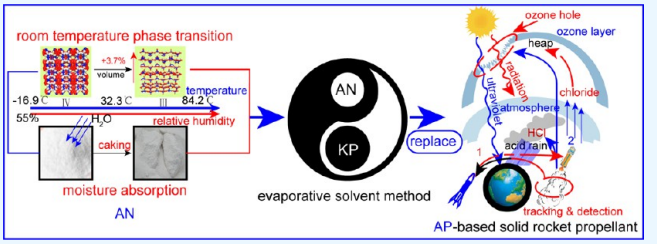

1. INTRODUCTION

High-energy-density energetic materials have emerged as a prominent research area within the field of high-energy materials. These materials possess a substantial amount of chemical energy stored within their molecular structure, and upon activation, they can release significant amounts of energy.[1] High-energy oxidizers play a crucial role in these materials and find extensive applications in propellants and military hybrid explosives. It is worth noting that high energy and low sensitivity are inherent trade-offs in such materials, thereby making energy and safety the two primary concerns in the field of energetic materials. Therefore, it is important to develop high-energy oxidizers with high density, high oxygen balance, high generation enthalpy, and low sensitivity.

The evaporative solvent method (ESM) is an important technique for improving material structure and is commonly used to prepare single crystal structures with minimal solubility changes at different temperatures. Slow evaporation of the solvent leads to the formation of crystals,[2] which are often utilized to enhance substance properties. For instance, the CL-20/TNT crystal reduces the mechanical sensitivity of the substance,[3] while the HMX/AP crystal decreases its hygroscopicity.[4] Apart from single crystal structures, the ESM is also employed to thoroughly mix two phases. When two solid-phase substances are mixed in a solvent, as the solvent evaporates, the two substances precipitate. The mechanisms involved include: (1) substitutional doping, where the ions of two substances exchange with each other, particularly in the case of inorganic substances; (2) surface adsorption, where one ion is attracted to another ion due to electrostatic forces; and (3) interstitial doping, where the layers of the substance can accommodate ions from another substance.[5]

Ammonium nitrate (AN) is one of the most important ammonium nitrogen compounds in industry and agriculture and is widely used in nitrogen fertilizers and explosives.[6] AN is the primary component of most industrial explosives and is also utilized as an oxidizer in military explosives and compound propellants. However, its moisture absorption and room-

Received: October 13, 2023
Revised: December 12, 2023
Accepted: December 13, 2023
Published: December 28, 2023

temperature phase transition restrict its widespread use. At atmospheric pressure, AN has five thermodynamically stable crystal structures in the temperature range of −17 to 170 °C, each of which exists only in a certain range. When the crystal structure changes, it is accompanied by a volume change, especially the IV ↔ III phase transition of AN, which is in the temperature range where AN is stored, transported, and used, with a volume change of 3.7%, which affects various properties of AN, such as mechanical strength, combustion properties, and explosive performance.[7] At the same time, it may also cause major safety accidents, such as on August 4, 2020, in the Lebanese capital, where a massive explosion in a warehouse storing 2750 tons of AN at the main port of Beirut nearly destroyed the entire city.[8] Nevertheless, AN is gaining more and more enthusiasm in the field of composite solid propellants and high-energy hybrid explosives with its low cost, environmentally friendly, smokeless, low susceptibility, and excellent blast performance.[9] Besides, ammonium perchlorate (AP), as a common oxidizer for propellants and military hybrid explosives, has become a fatal drawback due to its weak workability and environmental pollution problems.[10] Therefore, there is also an increasing interest in AN as an oxidizer to replace AP. The most important thing for AN to replace AP is to solve the phase transition and moisture absorption properties of AN.

Many researchers have worked on eliminating the room-temperature phase transition of AN. The addition of potassium salts is a common method to achieve phase stabilization of AN.[11] Most potassium salts can eliminate the existence of phase transition IV ↔ III when mixed with AN.[12,13] Besides, like oxides,[14] organometallic complexes,[15] composites,[16] and cellulose[17] can also inhibit the room-temperature phase transition of AN. In addition to the room-temperature phase transition, the strong moisture absorption of AN is a challenge that needs to be urgently overcome. Most research is focused on processes such as coating and surface modification,[18−22] whether it is to eliminate the room-temperature phase transition of AN by adding trace substances or to improve the moisture absorption of AN by coating or other means. However, these additives can be considered impurities in the AN system, which poses a challenge to the performance and safety of AN. This is not desirable. Unfortunately, current research cannot simultaneously address the two major shortcomings of AN improvement.

Cocrystallization is currently an effective way to modify energy-containing materials without destroying the original structure of the components but also combining the advantages of the two components together. For example, the AN/Benzo-18-crown-6 cocrystal not only changes the morphology of AN but also eliminates the disadvantages of the polymorphic transition near ambient temperature and the caking and smoke generation caused by the hygroscopic effect of AN.[23] Similarly, the HNTO/AN cocrystal study provides a new idea for the AN replacement of AP.[24] HNTO/AN high-energy cocrystal has good size distribution, uniform morphology, few defects, and high density. It does not exhibit any polymorphic transformation at ambient temperature. The obtained cocrystal is less sensitive than HNTO and close to the original AN. In addition, the developed cocrystal has higher activation energy and good thermal stability. The developed product has excellent energy content and good thermal stability, which can serve as a prominent oxidation system and has good applications in solid propellants and explosive formulations.[25−27] Another interesting example reported in the literature is the cocrystal of AN and potassium dinitramide (KDN) prepared by Kumar et al. using a ratio of 50/50.[28] It is demonstrated that KDN played an excellent phase-stabilizing role on AN and had a positive effect on the burning characteristics. This study demonstrates the feasibility of using catalytic AN/KDN + HTPB propellant formulations for green rocket propulsion. In terms of cost and safety, AN/KDN-based propellants are far superior to other available green oxidants. HTPB propellant based on AN/KDN (50/50) + Cu Co* is the most promising green propellant. If AN/KDN (50/50)-based oxidants are used together with other high-energy fuel adhesives such as GAP, or nanoscale Cu Co* as a catalyst or used together with other newly synthesized metal oxides, more effective propellant formulations can be obtained.[29] More recently, Oluwoye et al. prepared cocrystals of AN and saccharides and investigated their burning properties.[30] It is proved that such cocrystal displayed a low hygroscopicity and an energetically improved decomposition compared to pure AN and is stipulated to be a prominent ingredient for propellant formulations. Few studies have been reported on AN modification based on the cocrystallization technique, but there is no doubt that cocrystallization is a potentially valuable modification method.

KP, often widely used as an oxidizer in propellants and pyrotechnic agents,[31−33] has a higher density, higher oxygen balance, lower hygroscopicity, and lower sensitivity compared to AP, in addition to its relatively high burning rate, higher flame temperature, and higher effective propulsion. Pure KP has stable thermal behavior. It is worth mentioning that KP does not have the ability to explode, but with the addition of fuel, explosion can be achieved.[34,35] The introduction of the KP component for AN theoretically improves parameters such as density, oxygen balance, and combustion rate of the system.

In this present study, a series of novel high-energy MCCs were synthesized by ESM using AN and KP as coformers in order to overcome some drawbacks of AN and KP. Different characterization methods were used in order to better understand the formation mechanism of the MCCs. By using XRD, the crystal structures of the obtained high-energy MCCs were analyzed and compared. In addition, the AN, KP, and AN/KP MCCs were fully characterized by SEM, FT-IR, and DSC. In addition to this, the mechanical sensibility, moisture absorption properties, and explosion properties of the obtained products were evaluated. On the other hand, the apparent activation energies and finger front factors of different compounds were evaluated by applying kinetic models from nonisothermal DSC data to experimental DSC data using iterative Flynn-Wall-Ozawa (it-FWO) and iterative Kissinger-Akahira-Sunose (it-KAS). This study addresses the crystal phase transition problem of AN at lower temperatures by utilizing the MCC of AN and KP. The MCC substance formed shows significant improvements in hygroscopicity and thermal stability compared to AN. Additionally, the MCC substance exhibits lower friction and impact sensitivity, as well as enhanced explosive performance compared to AP. Overall, this research contributes to the expansion of the eutectic system in energetic materials and offers valuable insights for the selection and investigation of AP substitutes.

2. MATERIALS AND METHODS

2.1. Mixed Crystal Coprecipitation Preparation. AR-grade AN, KP, and AP were used for the experiments. The purpose of this study is to develop a substance that can potentially replace AP by utilizing the eutectic mixture of AN and KP. Taking into account the density of AP and aiming for a

https://doi.org/10.1021/acsomega.3c07979
ACS Omega 2024, 9, 1573−1590

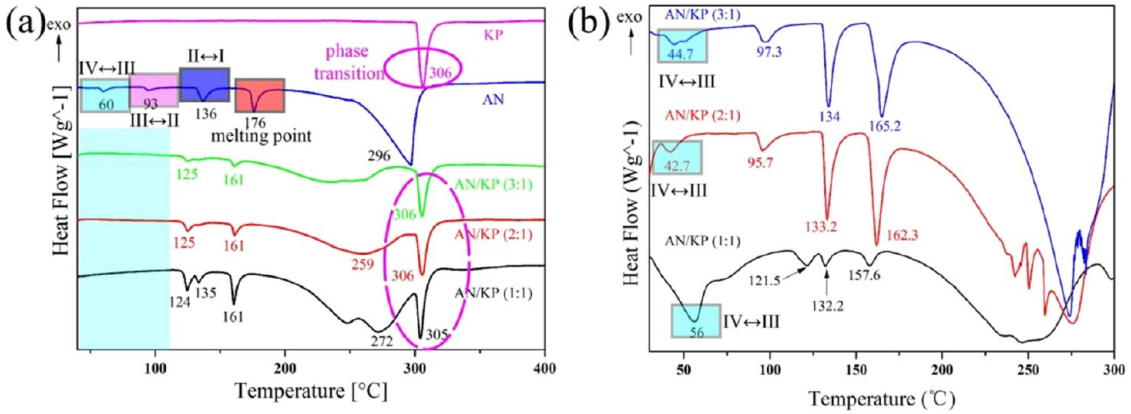

Figure 1. (a) DSC curves of experimental raw materials and crystalline samples with different molar ratios. (b) DSC curves of samples with different molar ratios under mechanical mixing conditions.

MCC material with improved explosive performance, we chose three MCC systems with theoretical densities higher than AP. These systems consist of AN and KP in molar ratios of 1:1, 2:1, and 3:1, respectively, and obtained three samples by solvent evaporation. In the preparation process of the sample with a molar ratio of 1:1, first, 1.385 g of KP was weighed and dissolved in 15 mL of water solvent. KP was completely dissolved at room temperature (note that the solubility of KP in water solution is much smaller than that of AN). Next, 0.804 g of AN was weighed and dissolved in the KP water solution. The beaker was then moved to a magnetic stirrer with a temperature set at 60 °C for evaporation. To prevent the loss of products during mixing, the reaction beaker was sealed with a preservative film, and the outlet of the water vapor was uniformly made to flow with pinholes. After the reaction lasted for 2 h, about 1/5 of the aqueous solution remained, and after the solution was cooled to room temperature, it was transferred to a vacuum desiccator for drying, and after drying was completed, it was stored in a desiccator for further analysis. Similarly, 0.6925 g and 0.4617 g of KP was weighed and dissolved in 10 and 5 mL aqueous solutions, respectively. Then, 0.804 g of AN was weighed and dissolved in KP aqueous solutions, and the preparation process was repeated for samples with a molar ratio of 1:1. The productivity of AN/KP eutectic is 93.4% (1:1), 91.5% (2:1), and 89.8% (3:1), respectively. In addition, the AN/KP MCCs may contain components such as raw materials AN, KP, hydroxylamine nitrate (HAN), and AN phase transitions, which will be analyzed in Section 2.3.

2.2. Mechanical Mixing Preparation. AN and KP were weighed again according to the proportions described inSection 3. The fixed proportions of AN and KP raw materials were poured into the mortar and milled at the same time, and after grinding for a certain period of time, sieving was carried out by using a 100-mesh standard sieve, and the sieved samples were sieved by using a 200-mesh standard sieve, and the particles with the samples in the 100−200 mesh range were selected as the raw materials for analyses. In order to ensure the reliability of the experimental data, three different molar ratios of mechanically mixed samples were obtained using the same steps.

2.3. Characterization of the Mixed Crystal Coprecipitation. X-ray diffraction data were obtained from a Bruker D8 Advance X-ray powder diffractometer, Cu target, $\lambda = 1.5046$ nm. FT-IR data were obtained by a Thermo Fisher IS5 Fourier transform infrared spectrometer with a resolution of 0.8 cm^{-1}. SEM images were obtained by the FEI Quanta 250 field emission scanning electron microscope.

The data for the thermal behavior studies of raw materials, MCCs, and mechanically mixed samples were obtained using a METTLER TOLEDO simultaneous thermal analyzer. The tests included an initial phase behavior study of the MCC samples as well as a phase behavior study after thermal cycling. Also, the thermal decomposition behavior between the hybrid crystals and the mechanically mixed material was compared. All tests were carried out in a nitrogen atmosphere, and the test samples were kept at the same level of dryness. The initial phase behavior of the MCCs and the mechanical mixtures was studied comparatively in the temperature ranging from 30 to 300 °C at a heating rate of 10 K/min, and the phase behavior after thermal cycling was studied at a heating rate of 5 K/min.

In order to further investigate the thermal decomposition of the prepared MCC samples, different heating rates of 5, 10, 15, and 20 K/min were employed to obtain the different DSC curves and TG curves. The kinetic parameters were calculated with DSC curves and compared with TG curves or DTG curves. It has been demonstrated in the literature that the isoconversion method provides more accurate results at multiple heating rates, so in this study, the Arrhenius parameters were calculated using the isoconversion method with the iterative Flynn-Wall-Ozawa (it-FWO) and iterative Kissinger-Akahira-Sunose (it-KAS).[36−39]

The moisture absorption characteristics of raw materials AN, KP, and three AN/KP MCC samples were determined by creating a constant humidity chamber with relative humidity (RH) of 50 and 90%, respectively, using aqueous sulfuric acid solution.

The impact sensitivity test was performed with a drop weight of 10 kg, a sample mass of 30 mg, and the impact sensitivity was expressed as H_{50}. The frictional sensitivity was tested using a BMA frictional sensitivity meter.

Based on the equilibrium reaction method, the explosion rates of raw materials AN, KP, and AN/KP MCCs were predicted using EXPLO 5 software, and the molar ratios of MCCs were converted into mass fractions when input. Then, a small-dose-based microexplosion test system was used to detect the detonation velocity of the samples, which consisted of a high-speed ripple shadow imaging module and a laser-induced plasma spectroscopy unit to test the detonation velocity from laser-induced shock wave images by a high-energy laser pulse

https://doi.org/10.1021/acsomega.3c07979
ACS Omega 2024, 9, 1573−1590

combined with a machine learning algorithm; the prediction error of explosive velocity was less than 4%.[40,41]

3. RESULTS AND DISCUSSION

3.1. Thermal Behavior. The raw materials AN and KP used in the experiments, as well as AN/KP MCCs with different molar ratios, were tested by TG-DSC coupling. The DSC results showed that there were three phase transition processes in the tested temperature range for the raw material AN with peak phase transition temperatures of 60, 93, and 136 °C, indicating the maximum heat absorption rates for α-rhombohedral crystals to β-rhombohedral crystals (IV ↔ III), β-rhombohedral crystal to tetragonal crystal (III ↔ II), and tetragonal crystal to cubic crystal (II ↔ I), respectively, and the maximum heat absorption rate of the crystalline phase transition (as shown in Figure 1a). The phase transition temperatures of pure AN and MCCs are shown in Table 1. Compared to previous studies, the onset phase transition temperature of each phase is elevated, which is related to the test equipment and test atmosphere, but the variation of the phase transition temperature is consistent and therefore does not affect the thermal stability analysis of the samples. The fourth peak indicates the melting peak of AN with a melting temperature of 176 °C. The fifth heat absorption peak indicates the decomposition peak of AN, which is completely decomposed in the temperature range of 176−296 °C. The raw material KP has only one heat absorption peak in the test range with a peak temperature of about 306 °C, which is a reversible crystalline phase transformation process of KP.

Table 1. Physical and Chemical States of Different Samples with Temperature Changes

	peak transition temperature (°C)				
sample	IV ↔ III	III ↔ II	new heat absorption peak	II ↔ I	melt point
pure AN	60	93		136	176
AN/KP (1:1)			124	135	161
AN/KP (2:1)			125	135	161
AN/KP (3:1)			125	135	161

The results of the study showed that AN/KP MCCs with different molar ratios have similar DSC variation patterns. The results show that the phase transitions of pure AN at IV ↔ III and III ↔ II are eliminated by AN/KP MCCs with different molar ratios, but the phase transitions of pure AN at II ↔ I and KP near 306 °C are retained by AN/KP MCCs, indicating that the phase transition paths of the samples are not changed. Meanwhile, the AN/KP MCC samples show a heat absorption peak that AN and KP do not have, with a peak temperature of about 124−125 °C. Besides, the melting point of AN/KP MCCs decreases to 161 °C. The appearance of the new heat absorption peak and the decrease of the melting point of the samples reflect the occurrence of bond energy-related molecular self-assembly between AN and KP. Accordingly, different molar ratios of AN/KP MCC samples exhibit similar physical and chemical properties, indicating that the form of interaction between AN and KP is determined.

To compare the effects of ESM and mechanical mixing method on AN/KP MCC, DSC tests were conducted on AN and KP mechanical mixtures with the same molar ratio as the samples obtained by the volatile solvent method. As shown in Figure 1b, the results in the figure demonstrate that when AN and KP are mechanically mixed in different ratios, the low-temperature crystal phase transformation of AN cannot be suppressed. In fact, the addition of KP even reduces the phase transition temperature of the system. The peak temperature for the crystal phase transition from IV to III in pure AN is 60 °C. However, when mechanically mixed with AN/KP in ratios of 1:1, 2:1, and 3:1, the peak temperatures for the characteristic phase transitions in AN decrease to 56, 42.7, and 44.7 °C, respectively. The melting points of AN/KP mechanical mixtures with different ratios are also lower than those of pure AN. Interestingly, unlike the samples prepared using the ESM method, the melting points of the mechanically mixed samples decrease further as the KP ratio increases. This suggests that KP promotes the decomposition of the system in the mechanical mixing process. On the other hand, the melting point of AN/KP MCC samples remains constant regardless of the component ratio, indicating that the structure of AN/KP MCCs is ordered and relatively uniform. Consequently, the results indicate that mechanical mixing is unable to eliminate or inhibit the low-temperature phase transformation of AN. On the contrary, it may actually promote decomposition.

The AN and AN/KP MCCs with different molar ratios were thermally cycled once between 20 and 100 °C, and then TG-DSC tests and analysis were performed, and the results are shown in Figure 2. After undergoing one thermal cycle, it can be seen from the DSC curve that the crystalline phase transition temperature of the samples is almost unchanged. The substances causing the mass loss of the samples may be HAN and water. Vargeese et al. showed that the presence of HAN raises the phase transition of IV ↔ III of AN, and after thermal cycling, the phase transition of IV ↔ III of AN falls back to near 30 °C.[11] In this study, however, the IV ↔ III phase transition of AN remained near 55 °C after one thermal cycle, indicating that HAN was not present in the AN sample. Because the preparation process and conditions remained consistent for all samples, the MCC samples also theoretically did not contain HAN, so the substance that caused the mass change was water. The thermal cycling results showed that AN as well as AN/KP MCCs did not lose their original crystalline phase behavior after one thermal cycle, indicating that the trace amount of water has almost no effect on the phase change process of AN and AN/KP MCCs.

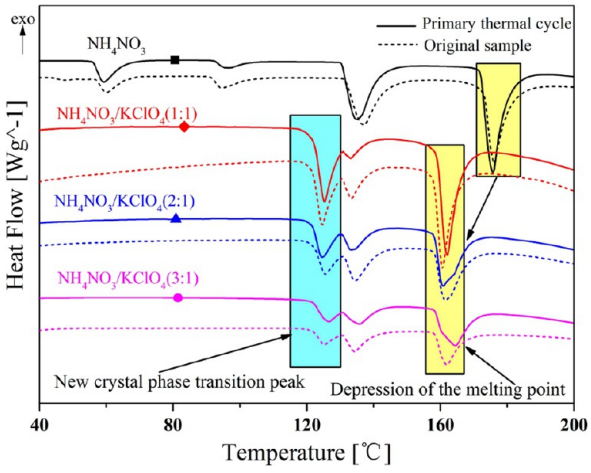

Figure 2. DSC curves of the original MCC samples and after one thermal cycle. @ indicates that a thermal cycle was experienced.

https://doi.org/10.1021/acsomega.3c07979
ACS Omega 2024, 9, 1573−1590

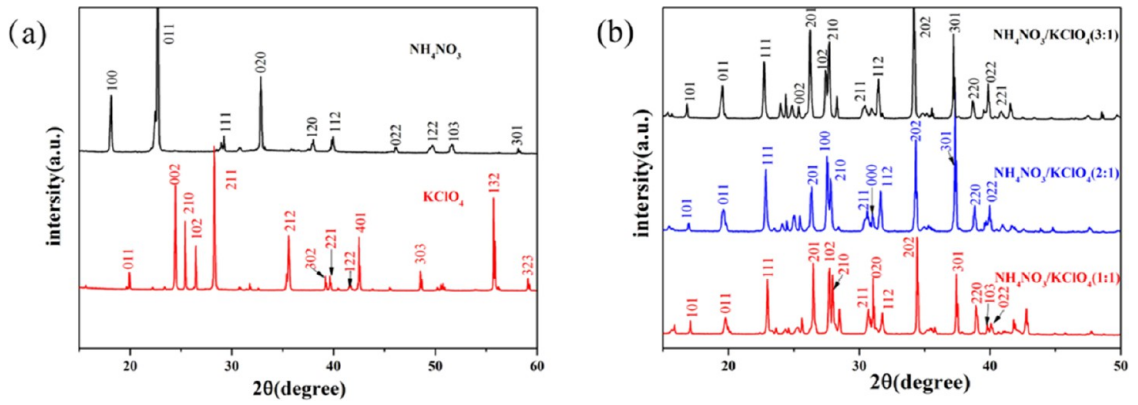

Figure 3. (a) XRD data of raw materials AN and KP; (b) XRD data of AN/KP MCC with different molar ratios.

In summary, AN/KP MCCs can effectively eliminate the phase transition of AN in IV ↔ III and III ↔ II, but the mechanical mixing method does not eliminate the phase transition of AN. Moreover, the phase behavior of AN/KP MCCs does not change after undergoing the thermal history from room temperature to 100 °C, and it has a good thermal stability in the temperature range of storage, transport, and use.

3.2. Crystalline Structure. The data of sharp peaks 3.91 (0 1 1), 2.72 (0 2 0), 4.88 (1 0 0), 3.05 (1 1 1), 2.25 (1 1 2), and 2.37 (1 2 0) Å of AN match with the JCPDS-ICDD database PDF#85-1093 matches, indicating that the raw material AN is in phase IV. The peaks observed in the XRD of the raw material KP are 3.16 (2 1 1), 3.64 (0 0 2), 1.65 (1 3 2), 3.50 (2 1 0), 2.52 (2 1 2), 2.13 (4 0 1), 3.37 (1 0 2), 1.87 (3 0 3), 4.45 (0 1 1), 2.27 (2 2 1), 1.56 (3 2 3) Å, etc., matched with PDF#70-0488 of the JCPDS-ICDD database. The XRD sample plots of raw materials AN and KP are shown in Figure 3a.

The XRD reflections of the AN/KP MCC samples are shown in Figure 3b. The results show that the AN/KP MCC samples with different molar ratios exhibit similar diffraction data, except for variations in the diffraction intensity of individual XRD peaks. Meanwhile, by comparing the diffraction data of AN, KP, and AN/KP MCC samples, it was found that despite the different molar ratios of AN/KP MCCs, the XRD diffraction data of pure AN and pure KP were not found in the XRD diffraction data of AN/KP MCC samples, indicating that AN and KP do not exist as a single component structure in the MCC samples with different molar ratios, which also verifies the previous statement that AN and KP exist in interaction.

An interesting thing was found by comparing the XRD diffraction data of AN/KP MCCs with the JCPDS-ICDD database search. The search results of AN/KP (1:1) MCC showed that $K_{0.093}(NH_4)_{0.907}NO_3$ (74-2050), NH_4NO_3 (76-1020), and $(NH_4)_{0.88}K_{0.12}NO_3$ (74-2051) are the main forms of AN/KP (1:1) MCC, and all three substances belong to the *Pnma* space group. Besides, there are also trace amounts of $KClO_4$ (76-1852, *Pnma*) and NH_4ClO_4 (70-2207, *Pnma*). The search results of AN/KP (2:1) MCC showed that $K_{0.093}(NH_4)_{0.907}NO_3$ (74-2050), NH_4NO_3 (76-1020), $(NH_4)_{0.88}K_{0.12}NO_3$ (74-2051), NH_4NO_3 (74-0972) with *Pbnm*, and $K_{0.2202}(NH_4)_{0.7798}NO_3$ (83-0726) are the main forms of AN/KP (2:1) MCC present. In addition, there are also trace amounts of $KClO_4$ (70-0488, *Pnma*) and NH_4ClO_4 (75-1130, *Pnma*); among them, the retrieved KP is consistent with the raw material used, while the retrieved NH_4ClO_4, although different from AN/KP (1:1) MCC, belongs to *Pnma*. The search results of AN/KP (3:1) MCC showed that $K_{0.093}(NH_4)_{0.907}NO_3$ (74-2050) and NH_4NO_3 (76-1020) are the main forms of AN/KP (3:1) MCC present. No detectable information on KP was found in the product, suggesting that NH_4ClO_4 became the main component in the mixed product. It is speculated that as the ratio of AN to KP increases, the K^+ ions in KP are completely occupied by the AN crystal cell, stabilizing the crystal phase. This speculation is supported by the DSC curve shown in Figure 1. When the AN to KP ratio is 3:1, the phase transition from II to I in AN begins to occur, indicating that the K^+ ion content at this ratio is insufficient to suppress the phase transition. These findings suggest an ion exchange mechanism between AN and KP when using the evaporation solvent method.

In addition to this, some trace amounts exist in the form of $(NH_4)_xK_yNO_3$ ($x + y = 1$). It is worth mentioning that AN exists in phase III in the AN/KP MCC samples, which is the reason why raw material AN (in phase IV) was not detected in the MCC samples. In addition to this, the retrieved results from the AN/KP MCCs show that the K^+ of KP partially replaces the NH_4^+ in AN, and the retrieved results are from the MCC of AN and potassium nitrate. Again, it shows that potassium salts act on AN in the same form, and the presence of K^+ in the AN cell is the main reason for achieving a stable phase of AN.

3.3. Chemical Structure Analysis. To further verify the existence of AN and KP interactions in the MCCs, FT-IR spectra of the raw material AN, KP, and AN/KP MCCs with different molar ratios were analyzed, and Figure 4 shows the FT-

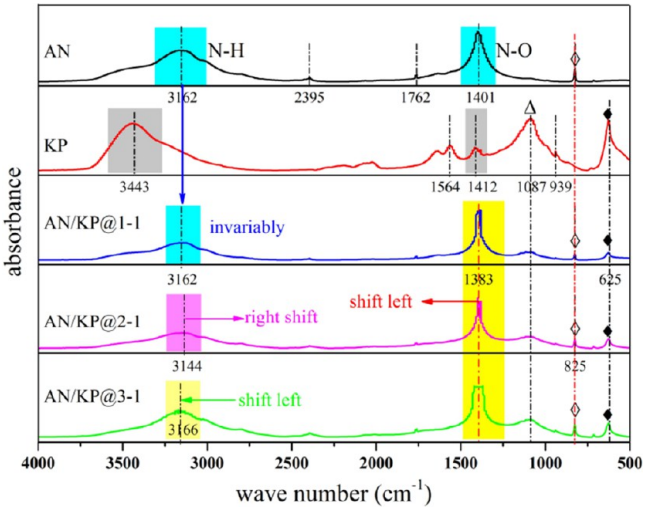

Figure 4. FT-IR spectra of raw material and MCC samples.

https://doi.org/10.1021/acsomega.3c07979
ACS Omega 2024, 9, 1573−1590

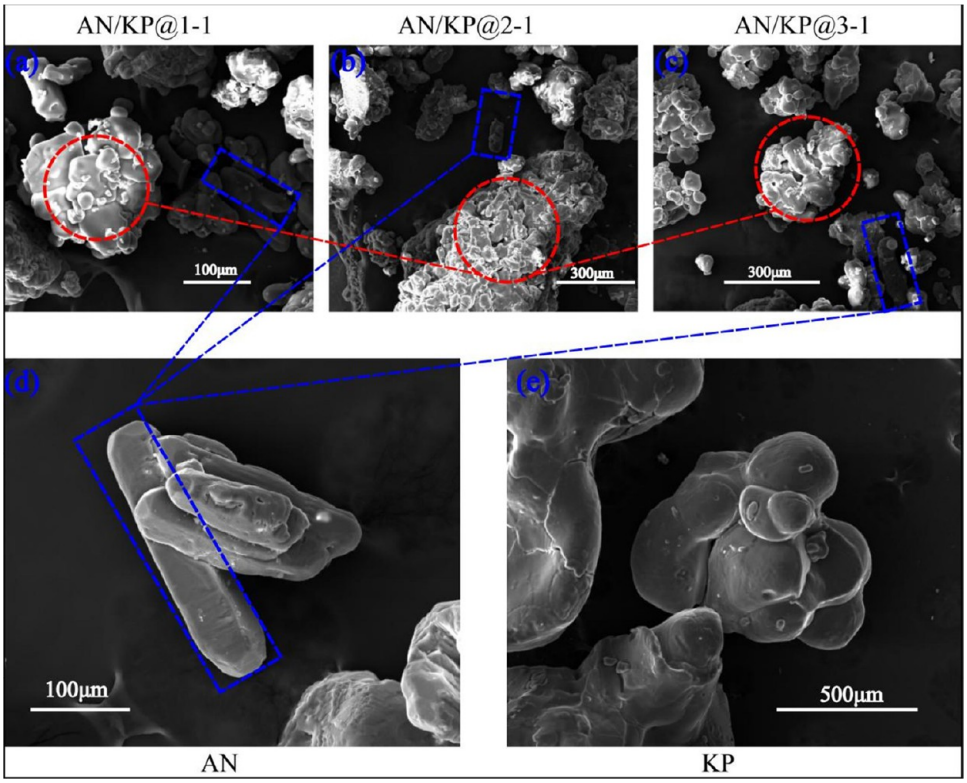

Figure 5. SEM of raw material and MCC samples. (a) AN/KP 1:1, (b) AN/KP 2:1, (c) AN/KP 3:1, (d) AN, and (e) KP.

IR patterns of the raw material and MCCs. The absorption of the MCCs is similar to that of the raw material AN, but some absorption peaks of AN and KP are significantly shifted; for the AN/KP MCCs, the absorption of AN at 3162 cm^{-1} is shifted to 3144 cm^{-1} for AN/KP (2:1) and 3166 cm^{-1} for AN/KP (3:1); the absorption at 1401 cm^{-1} is shifted to 1383 cm^{-1} for AN/KP (1:1), 1383 cm^{-1} for AN/KP (2:1), and 1383 cm^{-1} for AN/KP (3:1). The 3443 cm^{-1} absorption peaks of KP had disappeared. The FT-IR results indicate that there is indeed an interaction between AN and KP, and also verify the correctness of the results of the previous analysis.

3.4. Morphological Features of the Developed MCC. The SEM images of the crystals at different magnifications are shown in Figure 5. In particular, it is noted that the raw materials AN and KP were also recrystallized by the volatile solvent method in order to find the crystals of all samples nucleated and grown in the same environment. Because there were no single crystals in all samples prepared by the volatile solvent method, the samples analyzed by scanning electron microscopy were ground. The crystals of AN partially exhibited a complete single crystal structure, but most of them were incomplete, as shown in Figure 5d. The crystals of AN were polyhedral regular columns or bars. The recrystallized KP crystals are agglomerated or irregularly spherical with a smoother surface, but cracks are present, as shown in Figure 5e. To understand the growth patterns of AN/KP MCCs with different molar ratios, we photographed the surfaces of AN/KP (1:1) crystals (Figure 5 a), AN/KP (2:1) (Figure 5 b) crystals, and AN/KP (3:1) (Figure 5 c) crystals, respectively. The images show that the AN/KP MCCs with different molar ratios exhibit the same crystallographic growth pattern and are all formed by agglomeration of large and small particles with rounded structure, which do not have obvious single crystal structure in shape but are arranged in a consistent manner, and all have smooth crystal surfaces with similar grain sizes, which are distinctly different from those of the raw materials AN and KP.

The SEM results show that the grain growth patterns of the MCCs differ significantly from those of the raw materials AN and KP, mainly in terms of grain morphology and grain size. The crystal surface growth patterns of the MCCs with different molar ratios are consistent, and the crystal morphology and grain size are close to each other, indicating that the main phase components of the MCCs with different molar ratios are the same, which also illustrates the interaction between AN and KP in the solvent volatilization method and verifies that the interaction mechanism is the partial replacement of NH_4^+ in AN by K^+.

The AN/KP MCCs were characterized using analysis methods such as DSC, XRD, FT-IR, and SEM. It can be concluded that different proportions of substances have similar crystal and chemical structures, which is attributed to the ion exchange mechanism between the two substances. Research has shown that K^+ ions and NH_4^+ ions have similar orbital radii. When these substances dissolve in a solution, ions with similar atomic ion orbital radii will exchange, resulting in the formation of a solid solution. Additionally, the partial replacement of NH_4^+ ions by K^+ ions in AN enhances the hydrogen bonding effect and can eliminate the IV ↔ III phase transition of AN.[42−45]

The formation of AN/KP MCCs primarily relies on the exchange of positive and negative ions between the two substances in a specific proportion. This exchange leads to an equilibrium state through electrostatic attraction, as depicted in the figure. In the process, K^+ ions in KP partially substitute NH_4^+ ions in AN, resulting in the entry of K^+ ions into AN cells and the alteration of cell structure, thereby achieving phase stability. The presence of KP indirectly transforms AN from the IV phase to the III phase, allowing it to exist stably at room temperature. These findings demonstrate that AN/KP MCCs with varying

https://doi.org/10.1021/acsomega.3c07979
ACS Omega 2024, 9, 1573−1590

molar ratios can effectively inhibit AN. The phase stability mechanism of AN is illustrated in Figure 6.

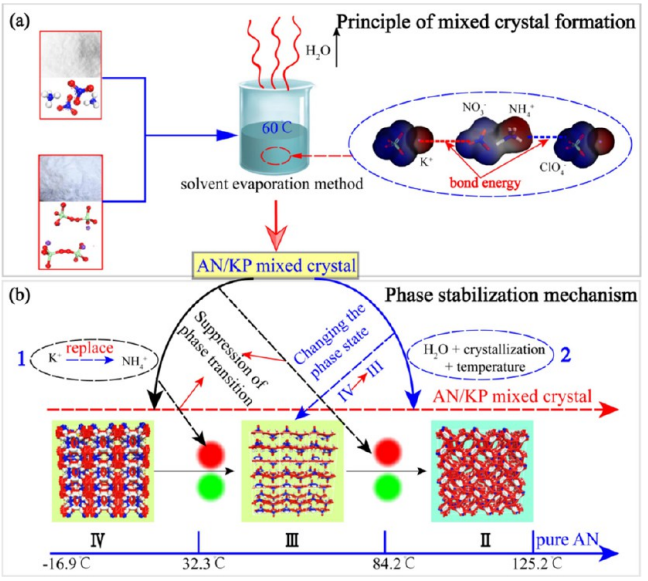

Figure 6. (a) Preparation of the AN/KP MCC process by ESM; (b) schematic diagram of the phase stabilization mechanism of AN.

3.5. Moisture Absorption Properties. The moisture absorption characteristics of the samples obtained using constant humidity solutions at different time intervals are shown in Figure 7. From Figure 7 a, it can be seen that all samples showed an overall trend of moisture loss at 50% RH, and the critical relative humidity (CRH) of AN was 55−60% at 30 °C. The pure AN lost the highest moisture within 12 h. With the passage of time, the pure AN and AN/KP (1:1) samples had alternating moisture losses between 12 and 48 h. At 48 h, pure AN lost more moisture than AN/KP (1:1), while AN/KP (2:1) and AN/KP (3:1) lost more moisture than pure AN. Pure KP showed a cyclic nature of moisture loss and moisture absorption at 50% RH. At 36 h, the saturation limit was reached for KP and 3 MCC samples, and this remained almost constant even after 48 h. However, the samples of pure AN continued to lose water. These observations can be explained by the fact that the crystals cocrystallized by the volatile solvent method may have retained the maximum amount of water. Since the nonrecrystallized pure AN samples did not lose the water present in the crystals, it took longer to reach the saturation limit for the pure AN samples than for the eutectic ones at 50% RH.

The moisture absorption characteristics observed at 90% RH (Figure 7b) are completely different from those observed at 50% RH, probably because this RH is much higher than the CRH of AN. At this point, the raw material KP reached the saturation limit at the beginning and basically did not absorb moisture during the subsequent process. All samples except KP absorbed moisture at 90% RH, but the absorption rate of pure AN was higher than that of the other three MCCs, which were between pure KP and pure AN, and increased as the molar ratio of AN increased. It can be seen from the SEM that the raw material AN is a rod-like crystal, while KP is a flat sheet-like crystal, which may give more surface for AN to absorb water. AN and KP molecules self-assemble into a specific structure, and KP partially accumulates on the surface of AN molecules, which prevents the intrusion of moisture. Therefore, the absorption rate of the three AN/KP MCCs is smaller than that of pure AN.

In summary, the moisture absorption characteristics of AN/KP MCC and pure AN at two different relative humidities have similar trends, but the moisture absorption characteristics at 90% RH are of more concern to us. At 90% RH, the moisture absorption capacity of each sample is: AN > AN/KP (3:1) > AN/KP (2:1) > AN/KP (1:1) > KP, compared with AN, the moisture absorption characteristics of AN/KP MCCs are substantially reduced.

3.6. Mechanical Sensitivity. The sensitivity of energetic materials is closely related to their manufacturing, transportation, and storage. To compare the sensitivity of raw materials and MCC samples, as well as MCC samples and AP, we conducted tests on the impact and friction sensitivity of raw materials (AN, KP, AP, and AN/KP MCCs). The test results, presented in Table 2, indicate that the impact sensitivity of AP is 13.72 J, whereas the impact sensitivity of AN, KP, and the three AN/KP MCCs is greater than 58.8 J. All samples exhibited a friction sensitivity greater than 360 N. Notably, the three AN/KP MCCs alloys demonstrated significantly lower sensitivity than AP, thereby ensuring enhanced safety and operability during production, storage, transportation, and use.

3.7. Explosive and Propellant Performance Prediction. The original purpose of developing AN/KP MCCs was to expand the application of AN in the field of composite propellants and hybrid explosives; therefore, it is necessary to accurately predict their explosive behavior and propellant properties. Explosive velocity is commonly used to characterize the explosive properties of a substance. The explosion velocities

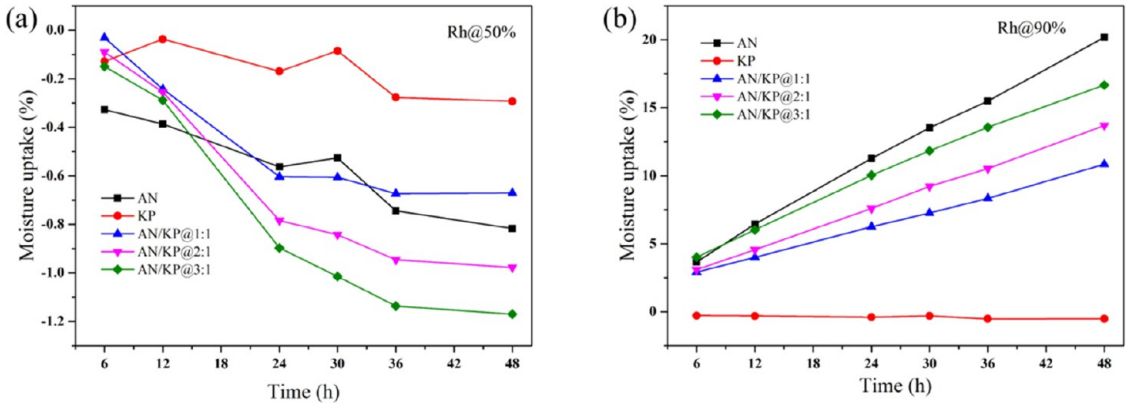

Figure 7. (a) Moisture absorption at 50%; (b) moisture absorption at 90%.

https://doi.org/10.1021/acsomega.3c07979
ACS Omega 2024, 9, 1573−1590

Table 2. Impact Sensitivity and Friction Sensitivity of Samples

sample	AN	KP	AN/KP (1:1)	AN/KP (2:1)	AN/KP (3:1)	AP
impact sensitivity H_{50}/J	>58.8	>58.8	>58.8	>58.8	>58.8	13.72
fraction sensitivity/N	>360	>360	>360	>360	>360	>360

calculated for each sample using EXPLO 5 software are shown in Table 3.

Table 3. Explosive Velocity of Each Sample Based on Equilibrium Reaction Method

samples	theoretical density/(g cm^{-3})	effective oxygen content /(%)	explosive velocity / (m s^{-1})
AN	1.72	20	7887
KP	2.52	46	nonexplosive bombardment
AN/KP (1:1)	2.15	37	5932
AN/KP (2:1)	2.02	32	6554
AN/KP (3:1)	1.95	30	6970

The explosive velocity calculated using EXPLO 5 tends to be ideal, and the actual explosive velocity of the difference is large, only as a reference; therefore, the determination of the sample explosive velocity is possible with the help of a higher prediction accuracy of the microexplosion test system. We obtained the samples by the microexplosion test system of the Schlieren images. As shown in Figure 8a, the Schlieren technique is a very traditional method to obtain the refractive index change of the fluid along the optical path and to analyze the temporal characteristics of the laser-generated plasma and shock waves. Figure 8a shows the Schlieren images of samples AN/KP (1:1), AN/KP (2:1), AN/KP (3:1), and AP with a delay time of 5 to 20 μs after laser ablation, indicating the temporal evolution of the laser-induced shock wave and the expansion of the plume into the ambient atmosphere. In the first frame, bright sparks obscure the front of the shock wave. Subsequently, after a delay of 5 μs, the decaying sparks and the semicircular shock wavefront are clearly visible. By comparing the images of each sample in Figure 8a, the differences in the microsecond evolution of the samples can be summarized in two points:

i. Sample AP has a brighter plasma at 5 μs.

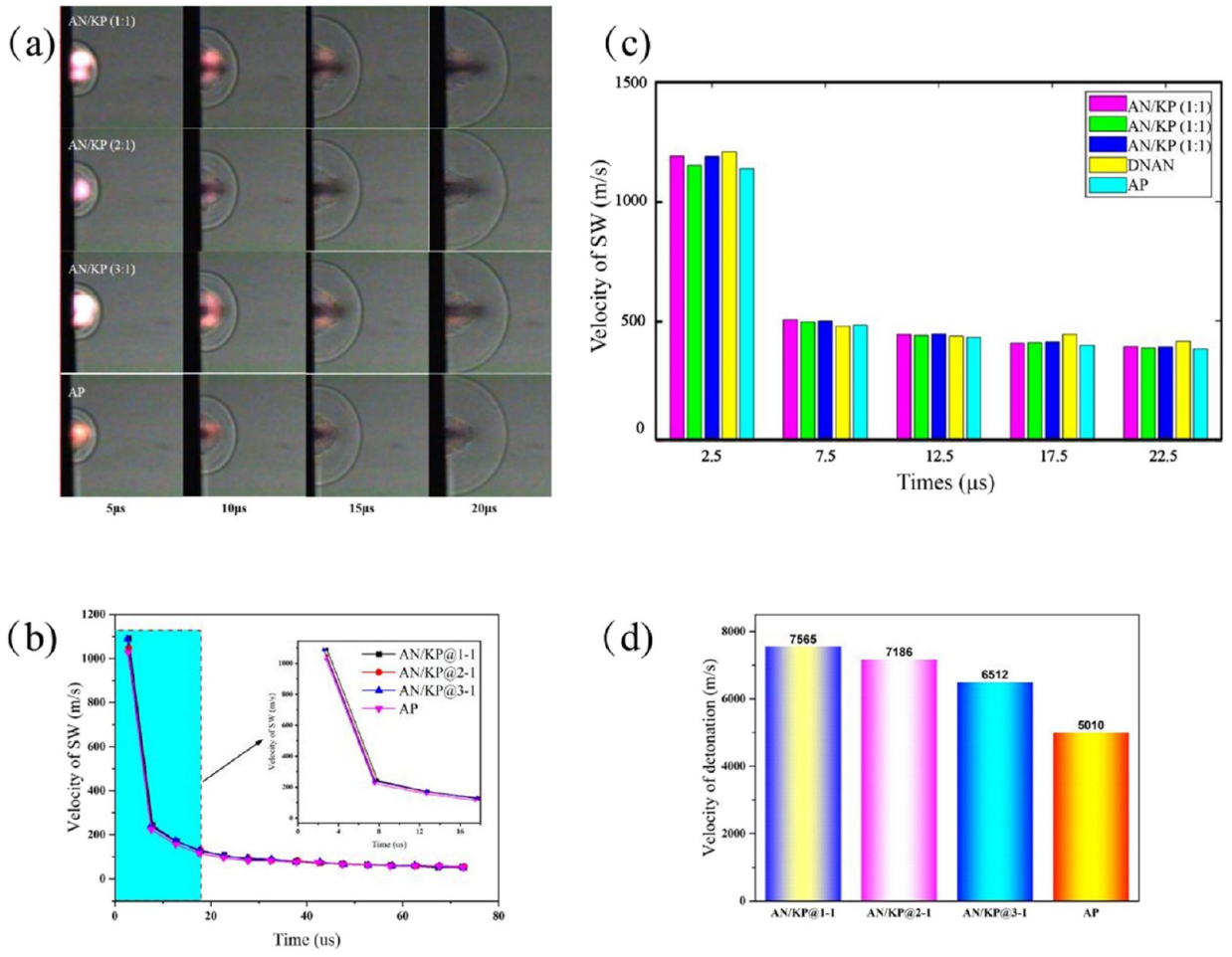

Figure 8. (a) High-speed Schlieren shots taken at different times after the onset of plasma formation of samples. (b) The variation curve of sample shock wavefront velocity with time. (c) Laser-induced shock wave velocity versus time for each sample with DNAN front. (d) Explosion velocity quantification of shock wavefront velocity.

https://doi.org/10.1021/acsomega.3c07979
ACS Omega 2024, 9, 1573−1590

Table 4. Comparison of Energy Parameters for Different Propellant Formulations

samples	HTPB/%	oxidizer/%		Al/%	T/K	I_{sp} /(M/SEC)	I_{sp} /(S)
1	14	AN	68	18	2729.24	2250.4	229.6
2		KP			3835.07	1921.8	196.1
3		AN/KP (1:1)			3403.89	2095.3	213.8
4		AN/KP (2:1)			3235.04	2153.1	219.7
5		AN/KP (3:1)			3128.35	2181.2	222.6
6		AP			3494.75	2332.4	238.0

ii. The shock wave propagation time of sample AP is slightly shorter and slower than that of sample AN/KP MCCs.

The plume of all samples is closer to that of the lower energy materials (images of the plume of lower energy materials can be found in the literature)[40,41] which consume more energy in luminescent radiation unrelated to the explosion, resulting in brighter radiation and lower explosive performance.

In order to quantify the explosive velocity of the samples, temporal features were extracted from the Schlieren images to obtain the shock wavefront velocity of the samples. This is shown in Figure 8b. By comparing it with the known samples in the microexplosion test system, the explosive velocity of the sample was found to be close to that of 2,4-dinitroanisole (DNAN), as shown in Figure 8c. After quantifying the velocity at the front of the shock wave, the results are shown in Figure 8d. It is evident that the explosion velocity of AN/KP MCCs is much higher than that of AP.

AN/KP MCC samples all have explosive capacity, but the explosive capacity varies slightly. Calculations for EXPLO 5 show that the explosive rate of AN/KP MCC with different molar ratios is significantly lower than that of the raw material AN. However, it is worth noting that, except for the monomers, different molar ratios of AN/KP are simply mixed in mass fractions, and various components are present as monomers in the mixture. In microexplosion tests, different molar ratios of AN/KP MCCs as well as AP exhibit the explosive characteristics of low-energy materials; the explosive velocity is close to that of DNAN explosives, but different molar ratios of AN/KP MCCs have significantly stronger detonation capacity than AP. This difference may arise from the formation of new cells or space groups due to the interaction of AN and KP in AN/KP MCCs, which changes the form of the presence of components.

The propulsive properties of oxidizers play a crucial role when used in solid propellants. In a similar manner, the propulsive performance of the oxidizer was assessed using EXPLO 5. However, the results indicated that the propulsive performance could not be determined solely for the oxidizer formulation. Therefore, a typical propellant formulation of HTPB/AP/Al was chosen to evaluate the propulsive performance of the AN/KP MCC oxidizer. Additionally, a comparative study was conducted with the feedstocks AN and KP. The performance of each propellant formulation is presented in Table 4.

Calculations indicate that the specific impulse of AN/KP MCCs as an oxidizer is positioned between AN and KP, leaning toward AN. However, the specific impulse of the propellant tends to decrease as the KP content increases. In comparison to AP, the three AN/KP MCCs exhibit higher densities and similar oxygen balances. Nevertheless, the specific impulse of the AN/KP MCCs is lower than that of AP. This disparity is primarily attributed to the presence of metal K ions in the oxidant of the AN/KP MCCs, leading to the formation of nonexclusively gaseous combustion products. Consequently, this factor impacts the specific impulse of the propellants. To enhance the specific impulse performance of the propellant, it is advisable to appropriately reduce the content of KP while ensuring that the oxidizer density and oxygen content remain within acceptable limits and the room-temperature phase transition is effectively suppressed.

3.8. Kinetic Analysis. The thermal stability of energetic materials is related to the safety performance of materials during storage, transportation, and use. In addition to characterizing their stability through thermal cycling experiments at a certain temperature, their stability is often assessed by studying their thermal decomposition behavior.

Solid-state processes are extensively studied by thermal analysis methods. Mechanisms of these processes are very often unknown or too complicated to be characterized by a simple kinetic model. They tend to occur in multiple steps that have different rates. To describe their kinetics, isoconversional methods are often used. The principal idea of the isoconversional methods is very simple; there are only two basic assumptions[46−49]:

1. Rate of the processes in a condensed state is generally a function of temperature and conversion:

$$\frac{d\alpha}{dt} = \Phi(T, \alpha) \quad (1)$$

The isoconversional methods employ the assumption that the function in eq 1 can be expressed as a product of two functions independent of each other, the first one, $k(T)$, depending solely on temperature T and the other one, $f()$, depending solely on the conversion of the process:

$$(T,) = k(T)f() \quad (2)$$

Combining eqs 1 and 2, the rate of the process can then be formally described by a single-step general rate equation

$$\frac{d\alpha}{dt} = k(T)f(\alpha) \quad (3)$$

The function $k(T)$ is usually considered to be the rate constant, and $f()$ is considered the conversion function, reflecting the mechanism of the process. The main implication of eq 3 is that the conversion function $f()$ at a fixed value holds for any temperature or temperature regime, i.e., the mechanism of the process is solely a function of conversion, it is not a function of temperature.

2. The activation parameters are obtained from a set of kinetic runs from the dependences of time vs temperature (for isothermal measurements), temperature vs heating rate (for integral and incremental methods with linear heating rate) or from reaction rate vs temperature (for the differential Friedman method). The evaluation is carried out at the fixed conversion.

https://doi.org/10.1021/acsomega.3c07979
ACS Omega 2024, 9, 1573−1590

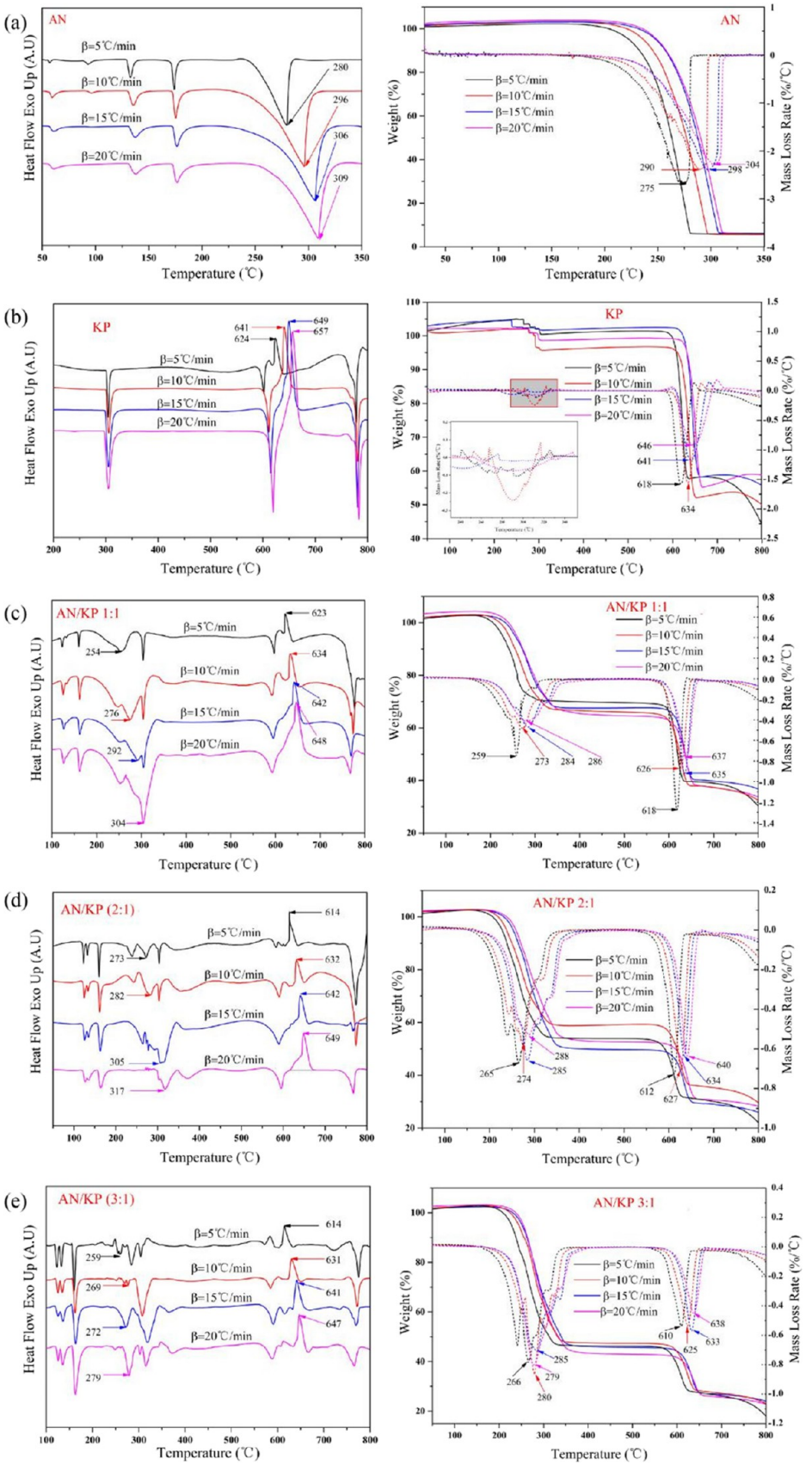

Figure 9. DSC, TG, and DTG curves of the samples. (a) AN, (b) KP, (c) AN/KP 1:1, (d) AN/KP 2:1, and (e) AN/KP 3:1.

Solid-state transformations are usually thermally activated, and $k(T)$ follows an Arrhenius dependence.

$$k(T) = A\mathrm{e}^{-E/RT} \quad (4)$$

https://doi.org/10.1021/acsomega.3c07979
ACS Omega 2024, 9, 1573−1590

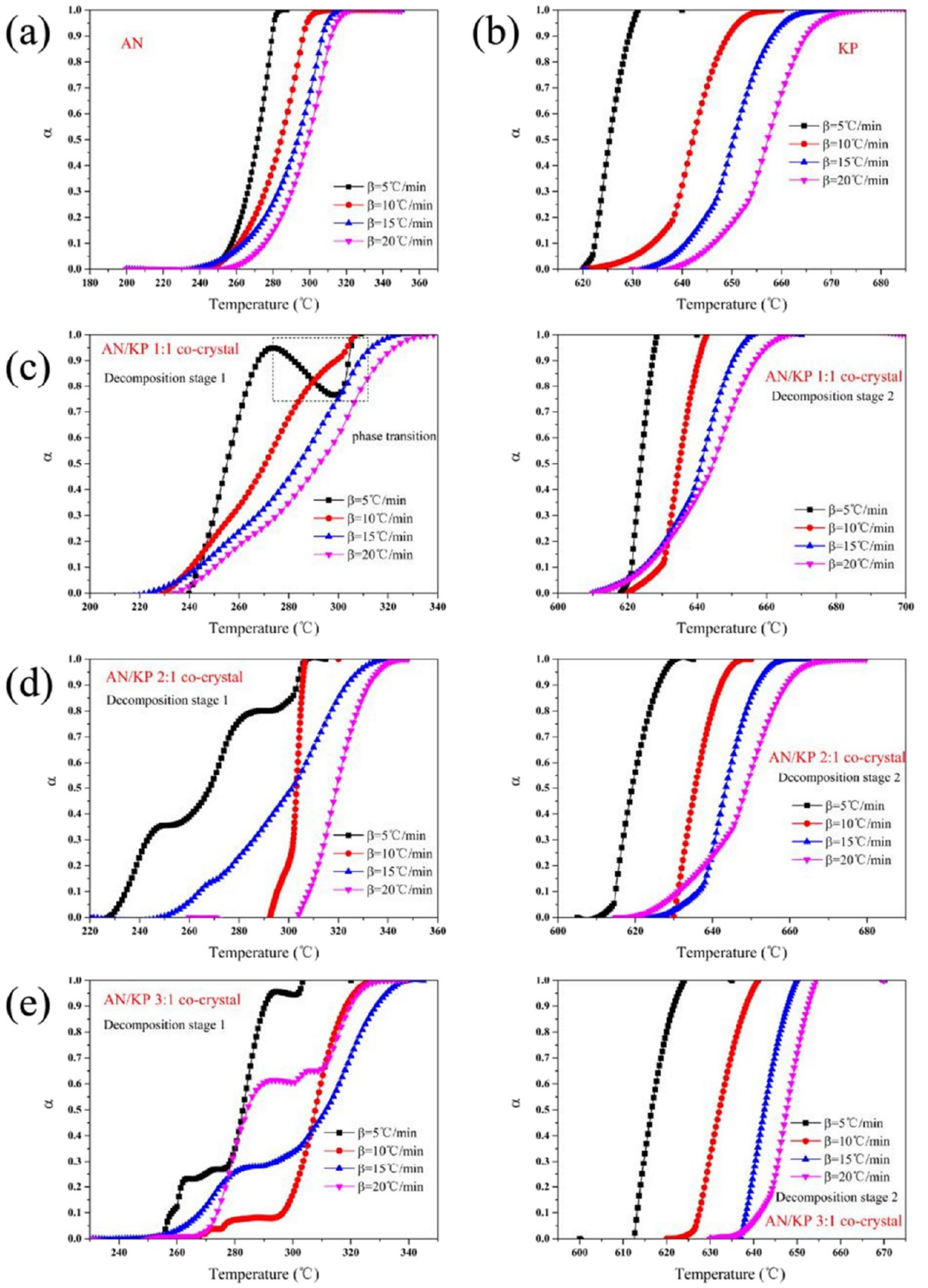

Figure 10. Variation of sample decomposition conversion rate as a function of temperature. (a) AN, (b) KP, (c) AN/KP 1:1, (d) AN/KP 2:1, and (e) AN/KP 3:1.

https://doi.org/10.1021/acsomega.3c07979
ACS Omega 2024, 9, 1573−1590

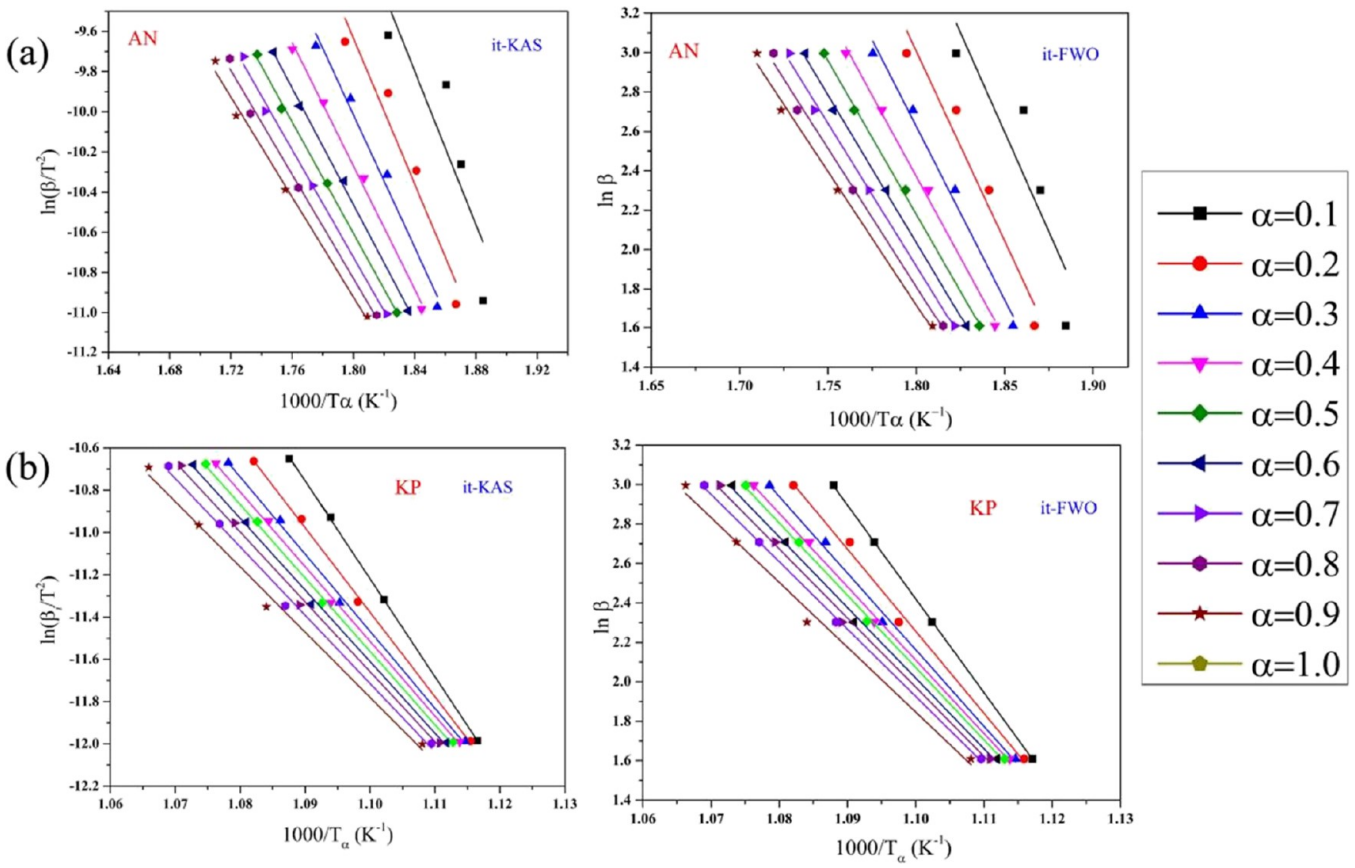

Figure 11. Linear fit of E_a and log A under the it-KAS and it-FWO methods. (a) AN and (b) KP.

where A is the pre-exponential factor, E is the activation energy, and R is the gas constant. For experiments carried out at a constant heating rate, the explicit dependence on time of eq 3 can be eliminated with

$$\frac{d\alpha}{dT} = \frac{1}{\beta} A e^{-E/RT} \cdot f(\alpha) \tag{5}$$

where $\beta = dT/dt$ = constant is the heating rate. Upon integration over the variables α and T, one can easily obtain the evolution of α. Applying isoconversional methods to continuous heating experiments relies on the determination of one or more of the system parameters (temperature, transformation rate,···) at which the same degree of transformation, a, has been reached for various heating rates, β. Then, activation energy for this degree of transformation, E_α, is obtained.

There are two calculation methods to be applied in this study. The Kissinger-Akahira-Sunose method (KAS) is an advanced method based on the Coats-Redfern approximation method (CR method), which can be written as follows:[50]

$$\ln\left(\frac{\beta_i}{T_{ai}^2}\right) = \ln\frac{A_a R}{E_\alpha} - \frac{E_\alpha}{R}\frac{1}{T_{ai}} \tag{6}$$

By the KAS method, the linear relationship between $\ln(\beta_i/T_{ai}^2)$ and $1/T_{ai}$ can be obtained for each extent of conversion. Then the activation energy of reaction can be calculated by the slope. When $E_a/RT_{ai} > 13$, the calculation results can be satisfied by applying the KAS method.

Moreover, the FWO method was developed based on Doyle's hypothesis by Flynn, Wall, and Ozawa. This is an isoconversional integration method, which can be expressed as follows[51]:

$$\ln\beta_i = \ln(0.0048 A_a E_\alpha)/g(\alpha)R) - 1.0516\left(\frac{E_\alpha}{RT_{ai}}\right) \tag{7}$$

β_i refers to the rate of temperature increase in K/min, T_{ai} is the peak temperature of the DSC curve at the rate of β_i increase in K, A_a is the prefactor, E_a refers to the activation energy in kJ mol^{-1}, R is the ideal gas constant, 8.314 J mol^{-1} K^{-1}, α is the depth of reaction, and $g(\alpha)$ is the integral form of the reaction mechanism function.

Eq 7 shows that for each conversion extent, lgβ_i can make a straight line with the slope $-0.1.0516E_a/RT_{ai}$ for $1/T_{ai}$, from which the activation energy at a specific conversion can be obtained.

The apparent activation energy (E_a) is the energy required for the reactants to overcome the energy potential barrier in order to initiate the reaction, while the exponential factor (log A) indicates the rate at which the reaction occurs. In fact, mixed crystal coprecipitation may affect the thermal and kinetic properties of the pure components, so E_a and log A must be determined simultaneously for both raw materials and derived MCCs.

Figure 9 shows typical DSC and TG curves of different samples, measured at different heating rates (β = 5, 10, 15, and 20 K/min). It can be seen that the different molar ratios of MCCs have similar heat absorption and exothermic processes, and there are two corresponding decomposition processes in the tested temperature range, with the stage 1 exhibiting heat absorption and the stage 2 exhibiting heat exotherm. With the increase in heating rate, the starting and peak temperatures shift to higher temperatures. It is worth noting that the decomposition steps of the eutectic samples become blurred and more

https://doi.org/10.1021/acsomega.3c07979
ACS Omega 2024, 9, 1573−1590

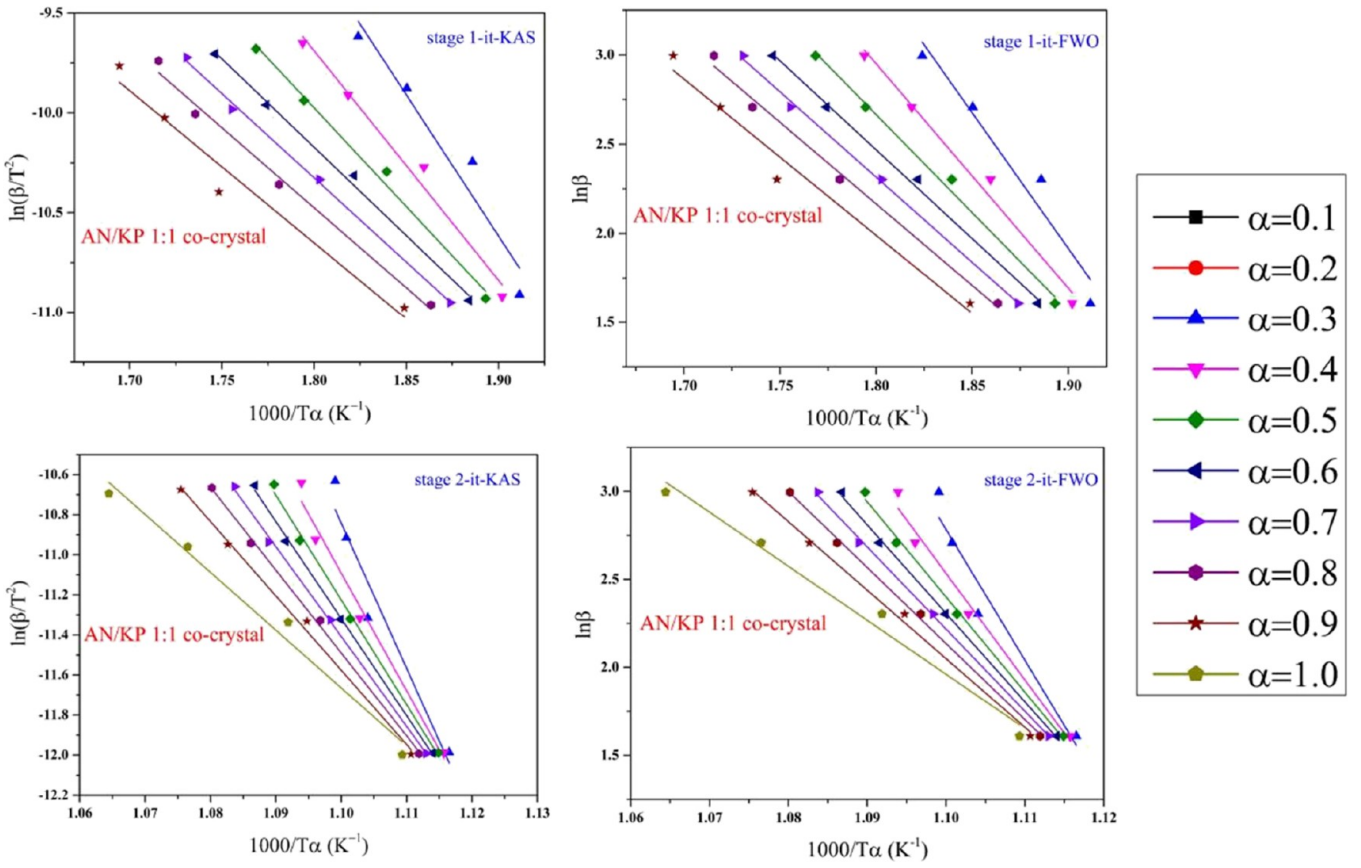

Figure 12. Linear fit of E_a and log A under it-KAS and it-FWO methods of AN/KP 1:1 MCC.

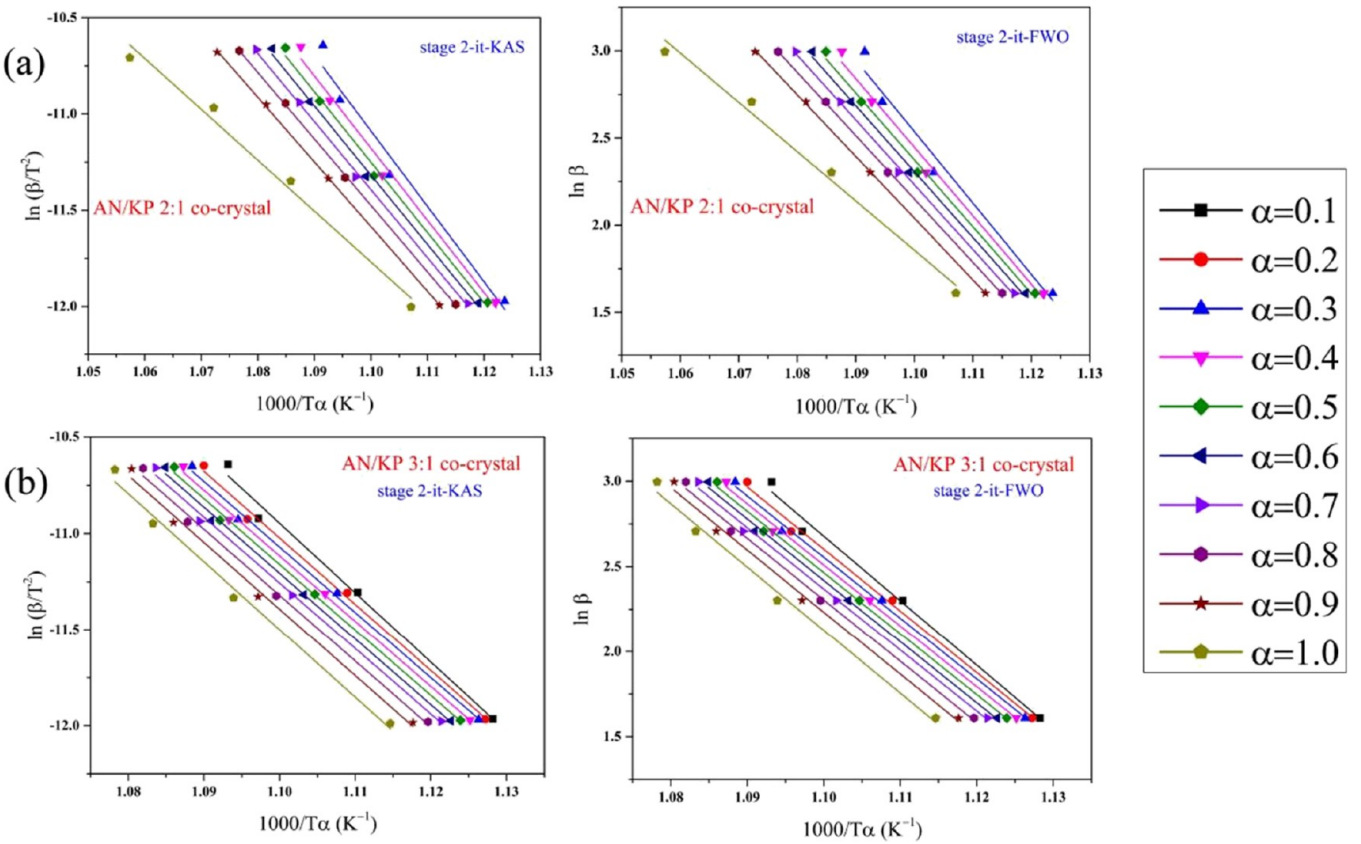

Figure 13. Linear fit of E_a and log A under it-KAS and it-FWO methods: (a) AN/KP 2:1 MCC, (b) AN/KP 3:1 MCC.

https://doi.org/10.1021/acsomega.3c07979
ACS Omega 2024, 9, 1573−1590

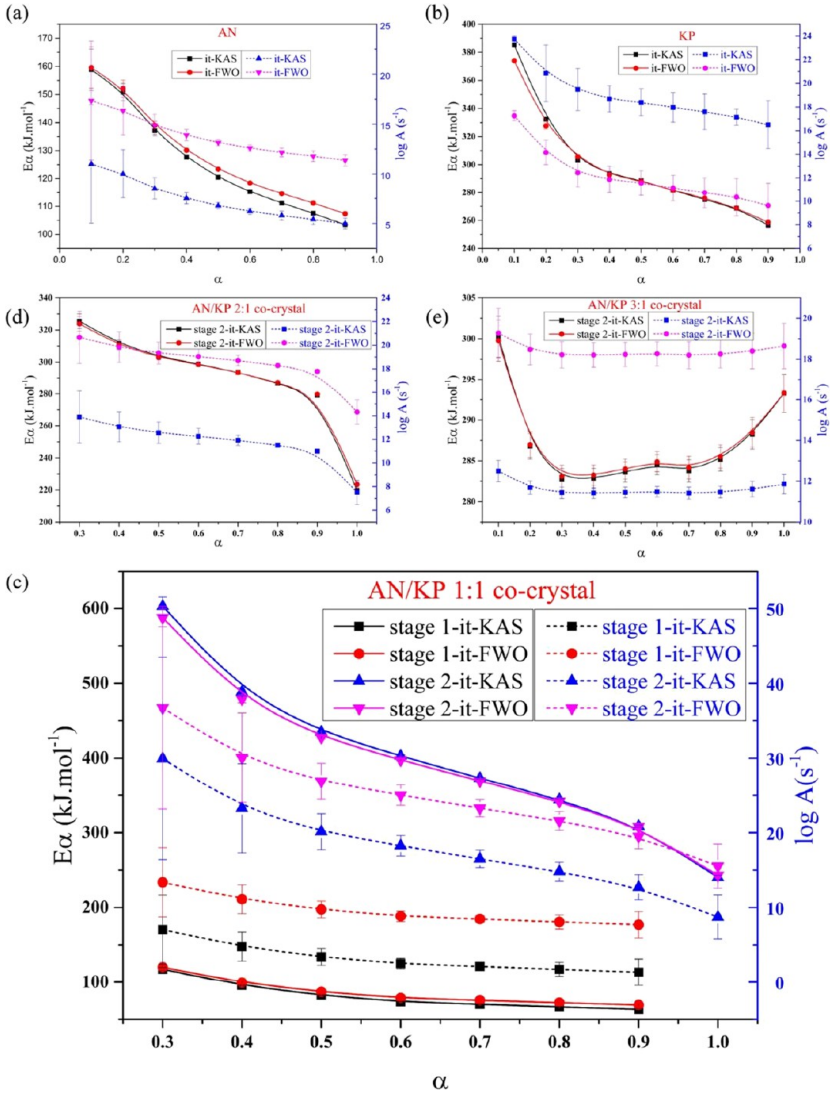

Figure 14. Variation of E_a and log A of the sample with conversion rate. (a) AN, (b) KP, (c) AN/KP 1:1, (d) AN/KP 2:1, and (e) AN/KP 3:1.

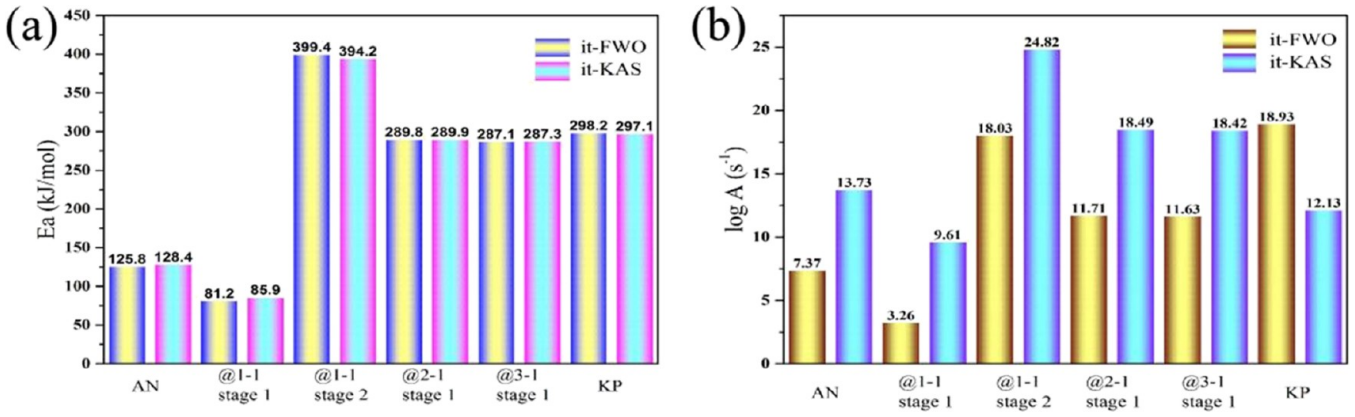

Figure 15. (a) Average E_a of samples, and (b) average log A of sample.

difficult to separate as the heating rate increases, and at the same time, the decomposition process of the prepared MCC material is mixed with the phase transition process; therefore, there is a certain error in the calculated E_a and log A.

When performing kinetic analysis, the conversion rate−temperature curve ($\alpha-T$) helps to understand more accurately the thermodynamic behavior of the sample during decomposition. Although there are many different reaction models, they can be classified into three main types, namely accelerated, decelerated, and s-shaped curves.[52] The transition temperature curves of the raw materials AN and KP can be considered S-shaped, similar to the second decomposition stage of each MCC

https://doi.org/10.1021/acsomega.3c07979
ACS Omega 2024, 9, 1573−1590

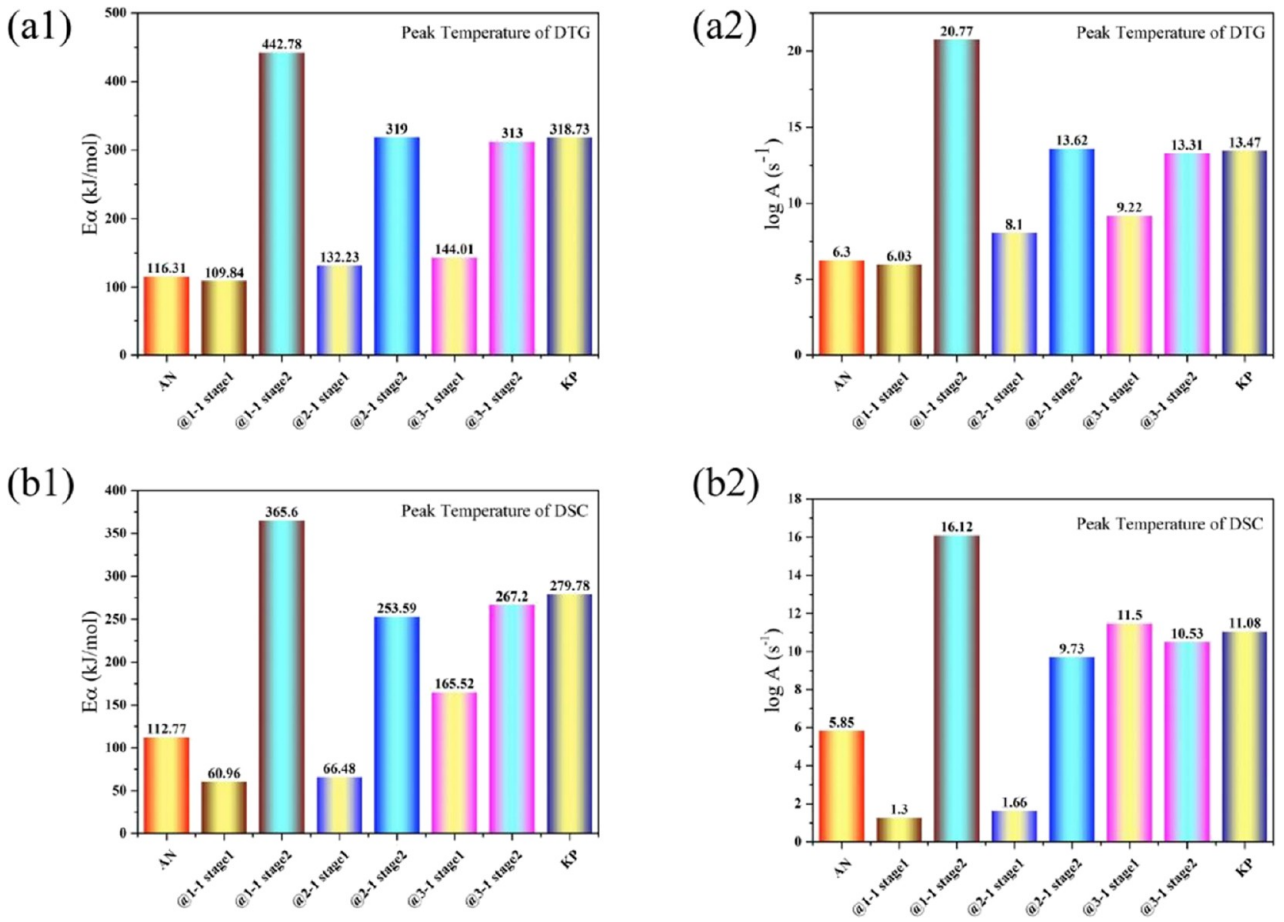

Figure 16. (a1) E_a at peak temperature based on DTG data, (a2) log A at peak temperature based on DTG data, (b1) E_a at peak temperature based on DSC data, and (b2) log A at peak temperature based on DSC data.

substance, while the first stage of the MCC substance has a more complex transition temperature curve, showing multiple S-shaped curves and acceleration curves accompanying the process, as shown in Figure 10. Therefore, for the solution of kinetic parameters, the thermal decomposition mechanism function is not considered in this study.

The $\alpha-T$ data were used as the basis for plotting against the it-KAS equation and the it-FWO equation. It-KAS method was plotted with $\ln(\beta/T_\alpha^2)$ vs $1000/T_\alpha$ and the it-FWO method was plotted with $\ln\beta$ vs $1000/T_\alpha$, as shown in Figures 11−13.

E_a and log A were obtained from the slope and intercept, and the results are shown in Figure 14. Figure 14 shows a plot of the dependence of activation energy versus conversion rate for the different studied samples using the two iso-inversion-free model methods. The apparent activation energy decreases with increasing conversion rates for AN and KP. For the studied MCCs, the evolution of E_a with conversion rate does not follow the same trend as for AN and KP. The differences in E_a values for these five substances further suggest the formation of a new compound. Both transition state theory and collision theory clearly indicate that log A is closely related to the activation entropy, suggesting that higher log A values imply the presence of significant active sites and a higher probability of collisions between reactants.[53] Based on the results obtained, it is possible to clearly check whether the calculated log A values of the samples differ, which is another piece of evidence confirming the formation of new compounds.

The mean values of E_a and log A are shown in Figure 15. The linear fit of this result has r^2 values in the range 0.9750−0.9999 and the results are of good quality. The E_a for AN is 125−129 kJ/mol, which is close to that reported in the literature.[54] The E_a for KP is 297−298 kJ/mol, which is consistent with the data reported in the literature.[55] The data reveals a significant difference in apparent activation energy between the raw materials AN and KP. From a reaction perspective, it is observed that the energy required for the molecular activation group reaction of AN is lower than that of KP, indicating that KP exhibits better thermal stability. Additionally, the consistency between the experimental data obtained in this study and the literature data suggests that the apparent activation energy data calculated using the it-KAS and it-FWO methods are reliable. This is further illustrated in Figure 15a. The AN/KP 1:1 MCC with an E_a of 81−86 kJ/mol for the stage 1 and 394−400 kJ/mol for the stage 2. As in the analysis of thermal behavior above, the two decomposition stages of MCCs represent the single component decomposition process following the dissociation of AN from KP as the thermal process proceeds; therefore, the E_a of the stage 1 of thermal decomposition of the MCC substance should be based on the raw material AN as the reference material, while the E_a of the stage 2 is based on the raw material KP as the reference material. From the results, the E_a of AN/KP 1:1 MCC is much higher than that of the raw material KP, while the E_a of AN/KP 2:1 and AN/KP 3:1 MCC are nearly equal and slightly lower than that of the raw material KP. The E_a of the 1:1 MCC decomposition of AN/KP in the first stage is

https://doi.org/10.1021/acsomega.3c07979
ACS Omega 2024, 9, 1573−1590

lower than that of the raw material AN, indicating that the energy required for decomposition is lower. However, the thermal stability of AN/KP 1:1 is lower than that of AN, and the energy required for decomposition in the second stage is much higher than that of KP, indicating that it is more difficult to decompose. Generally, similar decomposition processes are not favorable for the reaction. On the other hand, the 2:1 and 3:1 MCC compositions of AN/KP exhibit different characteristics compared to the 1:1 MCC. The energy required for the second stage of decomposition in the 2:1 MCC is measured to be 289−290 kJ/mol, while for the 3:1 MCC, it is 287−288 kJ/mol. These values are lower than those required for pure KP decomposition. It is worth noting that the energy required for the first-stage decomposition of the 3:1 AN/KP MCC is higher than that of AN, indicating that its thermal stability is better. Overall, the 3:1 AN/KP MCC has more advantages compared to the other two MCCs.

The linear fitting error for the stage 1 of thermal decomposition of MCC substances is large, so the peak temperature of the DSC and DTG curves was selected for this study as the characterization and comparison of the apparent activation energy of the stage 1 of thermal decomposition of MCC substances. As shown in Figure 16, taking the DTG curve as an example, the peak temperature is the temperature at the maximum decomposition rate. In this case, the apparent activation energy of AN is 116.31 kJ/mol, which is slightly lower than the average value, and the apparent activation energies of AN/KP 1:1, AN/KP 2:1, and AN/KP 3:1 MCCs are 109.84 kJ/mol, 132.23, and 144.01 kJ/mol, respectively. The apparent activation energy of the AN/KP 1:1 MCC is similar to that of the raw material AN, and it increases as the percentage of AN increases; log A has the same trend. The combination of E_a and log A shows that of the three molar ratios of AN/KP MCCs, the AN/KP 1:1 MCC has relatively good thermal stability.

4. CONCLUSIONS

A series of attractive AN/KP energetic MCCs with molar ratios of 1:1, 2:1, and 3:1 was successfully synthesized by ESM. The prepared compounds exhibit a different morphology from that of the raw material. The MCCs show an orderly stacking of AN and KP as raw materials. The AN/KP MCC with different molar ratios has similar growth patterns, uniform morphology, and a good size distribution. In addition, the energy of MCC does not have any polymorphic transition near ambient temperature compared to AN. This stems from the ion exchange between NH_4^+ and K^+ due to similar ionic radii.

The hygroscopicity shows that the hygroscopicity of the MCCs is between AN and KP and decreases with increasing the percentage of KP. The mechanical sensitivity shows that the obtained MCCs have a sensibility close to that of the raw material, AN, exhibiting extremely low mechanical sensitivity characteristics. Meanwhile, the explosive performance calculations and small-scale tests of the MCCs show that the MCCs have high density, high oxygen balance, and excellent burst performance, and they have propellant-specific impulse performance similar to AN. In addition, the developed MCC exhibits higher activation energy compared to AN, showing its good thermal stability. It is worth mentioning that the adopted method can be considered easy to produce new high-energy MCCs with low sensitivity and high energy on a large scale and quickly. In fact, it can be deduced that the prepared MCCs can meet the main requirements for the development of new high-energy and low-sensitivity explosive oxidizers, i.e., high density, high oxygen balance, high energy, good thermal stability, and low sensitivity, and AN/KP MCCs have good prospects in the application of oxidizers in solid propellants and military mixed explosives.

AUTHOR INFORMATION

Corresponding Author

Zhiyue Han − *State Key Laboratory of Explosion Science and Safety Protection, Beijing Institute of Technology, Beijing 100081, China*; orcid.org/0000-0002-8517-5760; Email: hanzhiyue@bit.edu.cn

Authors

Rongcai Zi − *State Key Laboratory of Explosion Science and Safety Protection, Beijing Institute of Technology, Beijing 100081, China*

Yue Yu − *Beijing University of Chemical Technology, Beijing 100029, China*

Cheng Wang − *State Key Laboratory of Explosion Science and Safety Protection, Beijing Institute of Technology, Beijing 100081, China*

Ximing Zhang − *China Safety Technology Research Academy of Ordnance Industry, Beijing 100053, China*

Xueyong Guo − *State Key Laboratory of Explosion Science and Safety Protection, Beijing Institute of Technology, Beijing 100081, China*

Jianhua Chen − *Science and Technology on Applied Physical Chemistry Laboratory, Xi'an 710065, China*

Xinrui Zhang − *State Key Laboratory of Explosion Science and Safety Protection, Beijing Institute of Technology, Beijing 100081, China*

Jun Yang − *State Key Laboratory of Explosion Science and Safety Protection, Beijing Institute of Technology, Beijing 100081, China*

Complete contact information is available at: https://pubs.acs.org/10.1021/acsomega.3c07979

Notes

The authors declare no competing financial interest.

ACKNOWLEDGMENTS

This work was supported by the Foundation of Equipment Preresearch Area (No. 80918020105), the Science and Technology on Applied Physical Chemistry Laboratory (No.W-DYX21614260202), and the Basic product innovation plan, National Natural Science Foundation of China (22178026), and State key Laboratory of Explosive and Science Technology of China (ZDKT23-01).The authors gratefully acknowledge the Analysis & Testing Center, Beijing Institute of Technology, for XRD, FT-IR, device preparation, and characterization.

REFERENCES

(1) Jiao, F.; Xiong, Y.; Li, H.; Zhang, C. Alleviating the energy & safety contradiction to construct new low sensitivity and highly energetic materials through crystal engineering. *CrystEngComm* **2018**, *20*, 1757−1768.

(2) Walsh, R. D. B.; Bradner, M. W.; Fleischman, S.; et al. Crystal engineering of the composition of pharmaceutical phases. *Chem. Commun.* **2003**, *2*, 186−187.

(3) Yang, Z. W.; Li, H. Z.; Huang, H.; et al. Preparation and performance of a HNIW/TNT cocrystal explosive. *Propellants, Explosives, Pyrotechnics* **2013**, *38* (4), 495−501.

https://doi.org/10.1021/acsomega.3c07979
ACS Omega 2024, 9, 1573−1590

(4) Levinthal, M. L. Propellant made with Cocrystals of Cyclotetramethylenetranitermine and Ammonium Perchlorate, US, US4086110A, 1978.
(5) Hocking, M. B. R. K.; et al. Tuning Catalyst Selectivity for Ammonia vs Hydrogen: An Investigation into the Co-precipitation of Mo and Fe Sulfides. *Inorg. Chem.* **2023**, *62* (24), 9379−9390.
(6) Tyc, A.; Niewes, D.; Pankalla, E.; Huculak-Maczka, M.; Hoffmann, K.; Hoffmann, J. Anti-Caking Coatings for Improving the Useful Properties of Ammonium Nitrate Fertilizers with Composition Modeling Using Box-Behnken Design. *Materials (Basel)* **2021**, *14*, 5761.
(7) Oommen, C.; Jain, S. R. Ammonium nitrate: a promising rocket propellant oxidizer. *J. Hazard. Mater.* **1997**, *A67*, 253−281.
(8) Yue, Y.; Gai, W.; Boustras, G. Exploration of the causes of ammonium nitrate explosions: Statistics and analysis of accidents over the past 100 years. *Safety Science* **2023**, *158*, No. 105954.
(9) Jos, J.; Mathew, S. Ammonium Nitrate as an Eco−Friendly Oxidizer for Composite Solid Propellants: Promises and Challenges. *Critical Reviews in Solid State and Materials Sciences* **2017**, *42*, 470−498.
(10) Chaturvedi, S.; Dave, P. N. Review on Thermal Decomposition of Ammonium Nitrate. *Journal of Energetic Materials* **2013**, *31*, 1−26.
(11) Vargeese, A. A.; Joshi, S. S.; Krishnamurthy, V. N. Use of potassium ferrocyanide as habit modifier in the size reduction and phase modification of ammonium nitrate crystals in slurries. *J. Hazard Mater.* **2010**, *180*, 583−589.
(12) Kaniewski, M.; Hoffmann, K.; Hoffmann, J. Influence of selected potassium salts on thermal stability of ammonium nitrate. *Thermochim. Acta* **2019**, *678*, No. 178313.
(13) Xu, Z.-X.; Fu, X.-Q.; Wang, Q. Phase Stability of Ammonium Nitrate with Organic Potassium Salts. Central European. *Journal of Energetic Materials* **2016**, *13*, 736−754.
(14) Sudhakar, A. O. R.; Mathew, S. Thermal behaviour of CuO doped phase-stabilised ammonium nitrate. *Thermochim. Acta* **2006**, *451*, 5−9.
(15) Asgari, A.; Ghani, K.; Keshavarz, M. H. Investigating the Effect of Copper(II) Coordination Compound with Azodicarbonamide Ligand on the Phase-Stabilization of Ammonium Nitrate. *Zeitschrift für anorganische und allgemeine Chemie* **2018**, *644*, 58−64.
(16) Asgari, A.; Ghani, K.; Keshavarz, M. H.; Mousaviazar, A.; Khajavian, R. Ammonium nitrate-MOF-199: A new approach for phase stabilization of ammonium nitrate. *Thermochim. Acta* **2018**, *667*, 148−152.
(17) Mousaviazar, A.; Keshavarz, M. H.; Hayaty, M. The effect of cellulose derivatives on the phase transition and thermal behavior of ammonium nitrate. *J. Therm. Anal. Calorim.* **2017**, *128*, 1049−1056.
(18) Elzaki, B. I.; Zhang, Y. J. Anti-hygroscopic surface modification of ammonium nitrate (NH_4NO_3) coated by surfactants. *Arabian Journal of Chemistry* **2020**, *13*, 3460−3473.
(19) Elzaki, B. I.; Yue Jun, Z. Relationships between structures of surfactants and their anti-hygroscopicity performance of ammonium nitrate particles. *Arabian Journal of Chemistry* **2020**, *13*, 7626−7636.
(20) Elzaki, B. I.; Zhang, Y. J. Surface modification of ammonium nitrate by coating with surfactant materials to reduce hygroscopicity. *Defence Technology* **2019**, *15*, 615−620.
(21) Gezerman, A. O.; Corbacioglu, B. D.; Cevik, H. Improvement of Surface Features of Nitrogenous Fertilisers and Influence of Surfactant Composition on Fertiliser Surface. *International Journal of Chemistry* **2011**, *3*, 3.
(22) Gezerman, A. O. A novel industrial-scale strategy to prevent degradation and caking of ammonium nitrate. *Heliyon* **2020**, *6*, No. e03628.
(23) Tan, L.; Xia, L.-H.; Wu, Q.-J.; Xu, S.; Liu, D.-B. Effect of urea on detonation characteristics and thermal stability of ammonium nitrate. *Journal of Loss Prevention in the Process Industries* **2015**, *38*, 169−175.
(24) Abdelaziz, A.; Tarchoun, A.; Boukeciat, H.; Trache, D. Insight into the Thermodynamic Properties of Promising Energetic HNTO·AN mixed crystal co-precipitation: Heat Capacity, Combustion Energy, and Formation Enthalpy. *Energies* **2022**, *15*, 6722.
(25) Abdelaziz, A.; Tarchoun, A. F.; Boukeciat, H.; Trache, D. Insight into the Thermodynamic Properties of Promising Energetic HNTO·AN Co-Crystal: Heat Capacity, Combustion Energy, and Formation Enthalpy. *Energies* **2022**, *15*, 6722.
(26) Hanafi, S.; Trache, D.; Mezroua, A.; et al. Optimized energetic HNTO/AN co-crystal and its thermal decomposition kinetics in the presence of energetic coordination nanomaterials based on functionalized graphene oxide and cobalt. *RSC Adv.* **2021**, *11*, 35287−35299.
(27) Hanafi, S.; Trache, D.; Meziani, R.; et al. Thermal decomposition and kinetic modeling of HNTO/AN-based composite solid propellant in the presence of GO-based nanocatalyst. *FirePhysChem.* **2022**, *2*, 315−322.
(28) Kumar, P. Advances in phase stabilization techniques of AN using KDN and other chemical compounds for preparing green oxidizers. *Defence Technology* **2019**, *15*, 949−957.
(29) Kumar, P.; Joshi, P. C.; Kumar, R. Thermal decomposition and combustion studies of catalyzed AN/KDN based solid propellants. *Combustion & Flame* **2016**, *166*, 316−332.
(30) Oluwoye, I.; Altarawneh, M.; Gore, J.; Dlugogorski, B. Z. Burning properties of redox crystals of ammonium nitrate and saccharides. *Combust. Flame* **2020**, *213*, 132−139.
(31) Pourmortazavi, S. M.; Zaree, A.; Mirsadeghi, S. Taguchi approach-assisted optimization of spraying in non-solvent process for preparation of potassium perchlorate nanoparticles. *J. Sol-Gel Sci. Technol.* **2015**, *76*, 510−518.
(32) Ji, X.; Liu, Y.; Li, Z.; Yu, Q.; Gao, Y.; Zhang, H.; Wang, L. Thermal behavior of Al/Zr/$KClO_4$ pyrotechnic compositions at high temperature. *Thermochim. Acta* **2018**, *659*, 55−58.
(33) Zhang, J. Y.; Guo, X. Y.; Jiao, Q. J.; Zhang, H. L.; Li, H. Analysis of the Thermal BehavioUr of CL-20, Potassium Perchlorate, Lithium Perchlorate and Their Admixtures by DSC and TG, Central European. *Journal of Energetic Materials* **2018**, *15*, 115−130.
(34) Soydan, A. S.; Dokmetas, H. S.; Cetin, M.; Koyuncu, A.; Kaptanoglu, E.; Elden, H. The evaluation of the role of beta-hydroxy fatty acids on chronic inflammation and insulin resistance. *Mediators Inflammation* **2006**, *2006* (5), 64980.
(35) Hussain, G.; Rees, G. J. Effect of additives on the decomposition of $KClO_4$. *Fuel* **1991**, *70* (12), 1399−1401.
(36) Genieva, S. D.; Vlaev, L. T.; Atanassov, A. N. Study of the thermooxidative degradation kinetics of poly(tetrafluoroethene) using iso-conversional calculation procedure. *J. Therm. Anal. Calorim.* **2010**, *99*, 551−561.
(37) Liqing, L.; Donghua, C. Application of iso-temperature method of multiple rate to kinetic analysis dehydration for calcium oxalate monohydrate. *J. Therm. Anal. Calorim.* **2004**, *78*, 283−293.
(38) Kumar, P.; Chandra Joshi, P.; Kumar, R.; Biswas, S. Catalytic effects of Cu-Co* on the thermal decomposition of AN and AN/KDN based green oxidizer and propellant samples. *Defence Technology* **2018**, *14*, 250−260.
(39) Sahoo, A.; Gautam, R.; Kumar, S.; Mohanty, K. Energy optimization from a binary mixture of non-edible oilseeds pyrolysis: Kinetic triplets analysis using Thermogravimetric Analyser and prediction modeling by Artificial Neural Network. *J. Environ. Manage* **2021**, *297*, No. 113253.
(40) Wang, X.; He, Y.; Cao, W.; Guo, W.; Zhang, T.; Zhang, J.; Shu, Q.; Guo, X.; Liu, R.; Yao, Y. Fast explosive performance prediction via small-dose energetic materials based on time-resolved imaging combined with machine learning. *Journal of Materials Chemistry A* **2022**, *10*, 13114−13123.
(41) Wang, X.; Liu, R.; He, Y.; Fu, Y.; Wang, J.; Li, A.; Guo, X.; Wang, M.; Guo, W.; Zhang, T.; Shu, Q.; Yao, Y. Determination of detonation characteristics by laser-induced plasma spectra and micro-explosion dynamics. *Opt Express* **2022**, *30*, 4718−4736.
(42) Xu, Z. X.; Fu, X. Q.; Wang, Q. Phase Stability of Ammonium Nitrate with Organic Potassium Salts. *Central European Journal of Energetic Materials* **2016**, *13* (3), 736−754.
(43) Kaniewski, M.; Hoffmann, K.; Hoffmann, Józef Influence of selected potassium salts on thermal stability of ammonium nitrate. *Thermochim. Acta* **2019**, *678*, No. 178313.

https://doi.org/10.1021/acsomega.3c07979
ACS Omega 2024, 9, 1573−1590

(44) Liu, T.; Dabin, L.; Xu, S.; et al. The effect of mixing methods on the phase transition of ammonium nitrate. *Sci. Technol. Energ. Mater.* **2017**, *78*, 5−11.
(45) Hong, W.; Peng, G.; Wu, S.; Wang, J.; Yang, Z.; Ru, T. Effect of Potassium Nitrate on Anti-Caking Performance of AN-based NPK Granular Compound Fertilizer. *Integr. Ferroelectr.* **2020**, *208* (1), 17−27.
(46) Simon, P. Isoconversional methods Fundamentals, meaning and application. *Journal of Thermal Analysis & Calorimetry* **2004**, *76*, 123−132.
(47) Roura, J. F. Isoconversional analysis of solid state transformations. *J. Therm. Anal. Calorim.* **2011**, *105*, 757−766.
(48) Farjas, J.; Roura, P. Isoconversional analysis of solid state transformations: A critical review. Part II. Complex transformations. *Journal of Thermal Analysis & Calorimetry* **2011**, *105* (3), 767−773.
(49) Farjas, J.; Roura, P. Isoconversional analysis of solid-state transformations: A critical review. Part III. Isothermal and non isothermal predictions. *J. Therm. Anal. Calorim.* **2012**, *109* (1), 183−191.
(50) Gao, X.; Jiang, L.; Xu, Q. Experimental and theoretical study on thermal kinetics and reactive mechanism of nitrocellulose pyrolysis by traditional multi kinetics and modeling reconstruction. *J. Hazard. Mater.* **2019**, *386*, No. 121645.
(51) Vyazovkin, S. Isoconversional Kinetics Thermally Stimulated Processes. *Macromol. Rapid Commun.* **2006**, *27*, 1515−1532.
(52) Vyazovkin, S.; Burnham, A. K.; Criado, J. M.; Pérez-Maqueda, L. A.; Popescu, C.; Sbirrazzuoli, N. ICTAC Kinetics Committee recommendations for performing kinetic computations on thermal analysis data. *Thermochim. Acta* **2011**, *520*, 1−19.
(53) Morokuma, K.; Eu, B. C.; Karplus, M. Collision dynamics and the statistical theories of chemical reactions. I. average cross section from transition-state theory. *J. Chem. Phys.* **1969**, *51* (12), 5193−5203.
(54) Kumar, P.; Joshi, P. C.; Kumar, R. Thermal Decomposition and Kinetics Studies of AN, KDN and Their Mixtures with and without Catalysts. *Cent. Eur. J. Energy Mater.* **2017**, *14* (1), 184−200.
(55) Lin, L. K.; Lee, J. S.; Hsu, C. K.; et al. The Thermal Decomposition Studies of Potassium Perchlorate with Graphite Powder. *Anal. Sci.* **1997**, *13*, 383−385.

https://doi.org/10.1021/acsomega.3c07979
ACS Omega 2024, 9, 1573−1590